# B and V CCD Photometry of Southern, Extreme Late-Type Spiral Galaxies

Lynn D. Matthews
Department of Physics & Astronomy, State University of New York at Stony Brook, Stony Brook, NY 11794-3800
Electronic mail: matthews@gremlin.ess.sunysb.edu

and

John S. Gallagher, III
Department of Astronomy, University of Wisconsin—Madison, Madison, WI 53706
Electronic mail: jsg@tiger.astro.wisc.edu

## ABSTRACT

We present B and V CCD aperture photometry for a morphologically-selected sample of forty-nine southern, extreme late-type spiral galaxies. All objects are moderate-to-low surface brightness Local Supercluster field galaxies that were detected previously in H I surveys. Our sample features objects that have optical luminosities, optical sizes, and H I masses which are at the low end for spiral galaxies. These objects are not a new class of galaxy, but are examples of a common type of spiral galaxy that has been under-represented in nearby galaxy samples.

We discuss the limitations of standard photometric techniques as applied to extreme late-type spirals, and adopt a simple method of characterizing the light distributions of such objects in terms of aperture magnitudes, colors, color gradients, "mean disk scales", and optical structure.

In many respects, the global properties of extreme late-type spirals are intermediate between irregulars and ordinary high surface brightness spiral galaxies. While our sample galaxies generally have regular structures and well-defined centers, some of the objects are very blue and/or have large gas fractions ($\frac{\mathcal{M}_{HI}}{L_V}\sim$3-9)—i.e. properties which have been traditionally associated with dwarf irregular galaxies. Several galaxies become *redder* with increasing radius, a trend which seems to be uniquely found in certain dwarf and very late-type disk galaxies. In addition, we find bars to be common in extreme late-type spirals.

Our sample exhibits a diverse array of structural properties and morphologies in galaxies with otherwise similar physical parameters (e.g., $M_B$, $\mathcal{M}_{HI}$, B–V). A number of the galaxies possess unresolved, point-like nuclei which may be related to low-luminosity AGNs or to M33-like compact nuclei. Finally, several of the galaxies show distinctive surface brightness "steps" in their disks, demonstrating that even small, late-type spirals can have multi-component disks.

## 1. Background

A number of recent studies have begun to explore sets of spiral galaxies which previously had remained largely absent from existing gaalxy catalogues due to observational biases. An important example is the low surface brightness (LSB) spirals. Following the study of Romanishin *et al.* (1982), several photometric studies of LSB spiral galaxies have appeared (e.g., Knezek 1993; McGaugh & Bothun 1994; Rönnback & Bergvall 1994; Sprayberry *et al.* 1995b; de Blok *et al.* 1995; Karachentseva *et al.* 1996; Vennik *et al.* 1996). These investigations have provided some of the first detailed photometric studies of LSB galaxies that are not dwarf irregular systems. They have brought attention to the fact that LSB disk galaxies span a wide range of Hubble types (e.g., Thuan & Seitzer 1979; Schombert *et al.* 1992), although they are predominantly late-type spiral and irregular galaxies.

Because LSB spirals tend to be gas-rich and appear "underevolved", studies of such galaxies have the potential to aid in our understanding of issues ranging from galaxy structure, formation, and evolution, to the origin of Lyman $\alpha$ absorbers and the faint blue galaxy population (see, e.g., Rao & Briggs 1993; Rao *et al.* 1995; Impey 1993; van der Hulst *et al.* 1993; Rönnback & Bergvall 1994). However, in order to address these questions, it is imperative to explore in more detail the full range of properties spiral disks encompass.

With the exception of Rönnback & Bergvall (1994), existing photometric studies of LSB spirals have focussed on northern objects, selected by optical surface brightness (e.g., McGaugh & Bothun 1994; de Blok *et al.* 1995) and/or within some range of H I masses (e.g., Knezek 1993). Due to a combination of selection factors, these authors have emphasized large (e.g., Knezek 1993; Sprayberry *et al.* 1995b) or moderately large LSB spirals (e.g., de Blok *et al.* 1995). In part this likely arises from the presence of the Virgo Cluster and nearby galaxy voids in the northern hemisphere; because of these features, northern field samples tend to be skewed toward either very nearby dwarf galaxies or larger, more luminous objects outside of the Local Supercluster. Few studies have focussed on populations of galaxies intermediate between recently discovered LSB spirals and existing samples of smaller, moderate-to-low surface brightness (MLSB) late-type galaxies within the Local Supercluster (e.g., de Vaucouleurs *et al.* 1981; Longmore *et al.* 1982).

In addition, it has been largely unrecognized that many small, MLSB galaxies exhibit spiral structure (e.g., Matthews & Gallagher 1993; van Zee *et al.* 1997; but see also van den Bergh 1966; Longmore *et al.* 1982). This is partly because such objects were entirely missed due to their low surface brightnesses and/or small angular sizes, or because the small, faint spirals which were part of existing samples were mistakenly classified as irregulars due to the lack of high-quality optical images from which better morphological classifications could be made. As a result, MLSB Scd-Sm spirals largely have been excluded from systematic studies of the spiral galaxy class even though such spirals may represent the most common type of gas-rich, organized, nearby disk galaxy (van der Kruit 1987).

In the current study we present photometry for such a sample of objects. Our sample includes

spiral galaxies which have mean disk surface brightnesses of $\bar{\mu}_B$ ∼23.3–25.6 mag arcsec$^{-2}$ and are which are, on average, physically smaller and/or less luminous than typical objects featured in other recent studies of LSB spirals. Hereafter we refer to these galaxies as *extreme late-type spirals*.

For the purpose of this study we define "extreme late-type spirals"[1] as "the lowest-luminosity, late-type disk galaxies which still exhibit regular optical structures and centralized light concentrations." In other words, these are Scd-Sm spirals which generally have mean surface brightnesses below those of normal spirals (i.e. below the night sky level) and which often fall at the low-end extreme for spiral galaxies in terms of properties such as H I mass, optical luminosity, and optical size.

Unlike other recent photometric studies of galaxies, we focus exclusively on a *morphologically selected* sample of Local Supercluster, extreme late-type spiral disks. By not applying a strict surface brightness, angular size, inclination, or H I mass cutoff to our sample, we find we have selected a group of MLSB spirals which both complements and extends past studies. For example, unlike some existing photometric studies, we have not excluded edge-on galaxies. Since dust obscuration in LSB galaxies may be low (e.g., Rönnback & Bergvall 1995; de Blok *et al.* 1995; Kodaira & Yamashita 1996), observed surface brightness will increase when LSB galaxies are viewed edge-on. Thus face-on samples might be biased in favor of the selection of higher luminosity galaxies (which are easier to find and classify) and against the selection of galaxies with the lowest intrinsic (i.e. inclination-corrected) central surface brightnesses, as such objects would become nearly invisible when viewed face-on.

Our sample includes many galaxies which, prior to CCD imaging, would have been called "irregular" or "peculiar" rather than spirals (cf. Tables 1 & 4), and includes some spirals with lower luminosities and/or H I masses than the spirals which typify recent LSB spiral samples (see e.g., Briggs 1997). Thus our sample helps to bridge the gap between past photometric studies of nearby Sm/Im systems such as the UK Schmidt photographic study of Longmore *et al.* (1982), the DDO dwarfs (de Vaucouleurs *et al.* 1981), extremely LSB Sm/Ims (Rönnback & Bergvall 1994) and larger LSB disks, which may be outside of the Local Supercluster.

As pointed out by McGaugh *et al.* (1995), morphological classifications for MLSB galaxies are more difficult than for HSB objects since features such as arm design (the main determinant of the assigned morphological type on the Hubble system) are not as pronounced in these dim galaxies. However, the darker skies of the southern hemisphere offer an extra advantage in discerning faint

[1]Commonly the term "late-type spiral" is used to encompass all spiral types Sbc or later, including small and giant spirals. To distinguish our sample objects as a special subset of late-type galaxies, we have adopted the nomenclature "extreme late-type spirals". We have avoided the use of the word "dwarf spiral", since there has been continual ambiguity in the literature as to whether this term implies some sort of luminosity cutoff, or instead denotes some set of structural properties (see Bingelli 1993). In addition, oftentimes "dwarf" is used to denote a galaxy that is not rotationally supported (e.g, Tully & Fouqué 1985); however, "dwarf spirals" *are* rotationally supported disks.

structures in MLSB objects; and based on their structural regularities and well-defined centers, our sample galaxies cannot be classified as irregulars. In addition, our sample galaxies tend to have pronounced radial surface brightness gradients, spiral-like H I profiles (see Fouqué *et al.* 1990; Gallagher *et al.* 1995; Matthews *et al.* 1997b), and in several cases, point-like nuclei (see Section 5.1.4). All of these features help to confirm the spiral-like nature of these objects. At the same time, however, lack of evidence for a bulge component in most cases (see Section 5.1.5) suggests that our galaxies are not early-type spirals (cf. Schombert *et al.* 1995).

In some ways our sample is heterogenous; it contains a range of arm designs, disk structures and thicknesses, and degrees of optical symmetry. Some of these spirals have low optical luminosities due to their very low surface brightnesses. Others have only moderately low surface brightnesses, but are still "underluminous" due to their small sizes. What these disks have in common is that they represent the range of possible galaxy "flavors" among the smallest and least luminous organized disk galaxies. As we discuss below, one of the intriguing features which unites these galaxies is that many have similar global physical properties in spite of their disparate optical morphologies.

## 2. The New Extreme Late-Type Spiral Sample

In total we present photometrically calibrated CCD images of forty-nine extreme late-type spiral field galaxies taken through Johnson B and V filters. The objects in our sample are listed in Table 1. None of these objects had previously existing photoelectric or CCD B and V photometry or published B–V colors. Our data were obtained as a part of a larger photometric survey (Gallagher & Matthews, in preparation) aimed at southern, late-type, MLSB field galaxies which had been catalogued as extreme late-type spiral or irregular galaxies by Corwin *et al.* (1985) or Arp & Madore (1987) and were subsequently detected in H I surveys of the Local Supercluster by Fouqué *et al.* (1990) or Gallagher *et al.* (1995).

These H I surveys uncovered many new moderately small H I-mass, Local Supercluster field galaxies ($\mathcal{M}_{HI}$~$10^8$–$10^9 M_\odot$) at distances between 10-40 Mpc. Previous H I surveys had been largely incomplete in the redshift range ($V_r$ <3000 km $s^{-1}$) and declination band (-18° < $\delta$ < −44°) of our study (Briggs 1997). A few additional targets for our optical survey were chosen from Tully (1988) or Kraan-Korteweg & Huchtmeier (1992); these were galaxies with late-type classifications (T=8-10) and with published H I data but no optical B and V photometry.

Our full imaging survey revealed that a surprisingly diverse array of optical properties exist among faint, moderately gas-rich, H I-detected nearby galaxies (e.g., Matthews & Gallagher 1993). From these data we were able to cull the subsample of objects having spiral-like properties that we present here.

## 3. New Data Acquisition

Our imaging data were obtained during the course of 7 nights at Cerro Tololo Inter American Observatory[2] in January 1993 using the 0.9m and 1.5m telescopes. All data were taken during dark time under photometric conditions and reduced using the standard IRAF[3] CCD reduction packages. The mean sky brightness for each image is listed in Table 3.

### 3.1. 0.9m Observations

We observed for 4 nights with the 0.9m f/13.5 telescope and Tek 512 CCD with the VEB controller. CCD readnoise was $\sim$7.7 $e^-$ and the gain was 4.28 $e^-$/ADU. Our plate scale was 0.445″ per pixel, and typical seeing was 0.7–1.3″. Due to our fairly small field of view (3.8′×3.8′) we focussed on galaxies whose catalogued diameters were less than 1.5′ for the 0.9m observations. Exposure times were 600 seconds in B and 900 seconds in V.

The data were bias subtracted using a median of 25 bias frames taken each afternoon and were flatfielded by dividing by a median dome flat and by a median twilight sky flat in the appropriate band.

### 3.2. 1.5m Observations

We observed for 3 nights with the 1.5m telescope, Tek 1024 CCD, and VEB controller. CCD readnoise was $\sim$3.8 $e^-$ and the gain was 2.97 $e^-$/ADU. We used the f/7.5 secondary which yielded a field of view of 7.2′ per side and a plate scale of 0.434″ per pixel.

We found the counts in the overscan strip of the Tek 1024 to be, on average, 7 counts higher in our flatfield frames than in our object frames. Due to this apparent dependence of overscan level on total image counts, no overscan correction was applied. A bias correction was performed by simply subtracting a median of 25 afternoon bias frames.

We found that small-scale structure was introduced by directly dividing by a median dome flat, so we produced a a modified dome flat by dividing the median afternoon dome flat by a 15×15 pixel median smoothed domeflat taken through the appropriate filter. Since our twilight sky flats appeared stable from night-to-night, we averaged the twilight flats from the three nights together to increase signal-to-noise. A 21×21 pixel median smoothing was applied to remove stars, and

---

[2]Cerro Tololo Inter-American Observatory is operated by the Association of Universities for Research in Astronomy, Inc. under contract with the National Science Foundation.

[3]IRAF is distributed by the National Optical Astronomy Observatories, which is operated by the Associated Universities for Research in Astronomy, Inc. under cooperative agreement with the National Science Foundation.

finally the domeflat-corrected images were divided by this median-smoothed twilight sky frame. Exposure times for each galaxy were 500 seconds in both B and V. Seeing ranged from 0.9-1.5″.

### 3.3. Photometric Calibration

Photometric solutions for our observing run were determined by monitoring several standard stars throughout each night. Aperture photometry was performed on the standard stars using the IRAF "apphot" package. Since all nights were photometric, we combined all of our 0.9m standard star data to produce a global photometric transformation solution for all four nights. Similarly, we combined the three nights of 1.5m data to solve for a single solution. We used linear transformation equations from which we obtained zero points, color terms, and extinction coefficients for the data from each telescope. Only the B–V transformation had an appreciable color term. Most of the scatter in the global solution comes from variable atmospheric extinction, as evidenced by the night-to-night variation in the derived extinction coefficient. Since we believe that extinction variations throughout each night and in different regions of the sky were comparable to the scatter in the night-to-night solutions, we have adopted the mean extinction coefficients from our global solution. Our transformation equations are presented in Table 2.

### 3.4. Galaxy Photometry

#### *3.4.1. The Problems of Surface Photometry of Late-Type and Low Surface Brightness Galaxies*

Accurate galaxy surface photometry is a complicated problem both in practice [e.g., choices of model parameters, dependence of derived parameters on signal-to-noise of data (e.g., de Vaucouleurs 1977)] and in terms of one's ability to derive a characterization of a galaxy's optical light which can be interpreted in a physically meaningful manner (e.g., in cases where the galaxy has non-elliptical isophotes or a significant asymmetry).

Traditionally, galaxy surface photometry involves fitting a series of elliptical isophotes to an image and from this extracting a magnitude and surface brightness profile based on the azimuthally averaged fit (e.g., Kodaira *et al.* 1990). Several authors have pointed out the shortcomings of this technique for characterizing a galaxy's true nature (e.g., Burstein 1979; Kent 1984,1985; Odewahn 1991; Tully *et al.* 1996). Moreover, the quantities derived from functional fits to the derived mean radial surface brightness profiles vary considerably between observers (Knapen & van der Kruit 1991).

We found multiple isophotal fits to be largely unsuitable for efficiently photometering the types of galaxies in our present sample. Instead we adopt a simple photometric approach based on simulated multiple aperture photometry and present a collection of optical measures of extreme late-type spiral galaxies which are free from model-dependent assumptions. We also provide

comments on interesting features of individual objects in order that our sample can be used to select galaxies for follow-up studies, where more more detailed examinations of the light distributions can be made (e.g., to complement 2-D kinematic data).

### *3.4.2. Photometry of the Extreme Late-Type Sample: The Procedure*

Our basic approach to photometering our galaxies was to use the IRAF/STSDAS "ellipse" package to fit a series of three concentric elliptical apertures to each object. The outmost ellipse allows us to determine a limiting isophotal magnitude, inclination, position angle, and axial ratio. The two additional ellipses provide a characterization of the light distribution of the galaxy in the nuclear region and a middle disk region, plus a coarse measure of the color gradient and the steepness of the surface brightness profile across the disk. Following, we outline the steps of our procedure and discuss our motivation for this approach.

1. A mean sky value for each B and V frame was determined by measuring the mean value in 3-6 rectangular regions, 15 or more pixels on a side. These regions were chosen as near as possible to the center of the chip while still avoiding contamination from stars or the diffuse light of the galaxy. The average of these measurements was subtracted from each respective frame.

2. Foreground stars and cosmic rays within the galaxy aperture were removed by replacing circular regions of an appropriate radius with an interpolation of the surrounding pixels as measured in an annulus surrounding the masked region. We used H$\alpha$–R frames of the galaxies when available (Matthews & Gallagher, unpublished) to distinguish foreground stars from H II regions within the galaxy. In a few images where the galaxy was contaminated by very bright stars with large diffraction spikes, complete removal of the starlight was difficult and photometric uncertainties are therefore larger; we have noted these cases in Table 3.

3. The center of each galaxy was found by simply locating the pixels of maximum light concentration. This location generally could be unambiguously located to within 2-3 pixels (i.e., the typical size of our seeing disk).

4. The length of the semi-major axis and its position angle were measured on each V frame, and an ellipticity was estimated from the measured major to minor axis ratio.

5. Using the estimated ellipse parameters, the outmost ellipse was fit to the galaxy. (The V-band surface brightness of the outermost fitted ellipse for each galaxy is listed in Table 3). Small adjustments were made to the ellipse parameters until a best-fit ellipse was found to the outer galaxy isophote. The validity of these fits were verified on several independent passes through the data in which the data were displayed using alternate scalings and color tables to emphasize faint details. For some of the faintest objects we smoothed the images and again checked by eye the goodness of our outer ellipse fits.

6. Once the outermost ellipse parameters were established, two additional ellipses were fitted at $\frac{a}{1.8}$ and $\frac{a}{(1.8)^2}$, where "$a$" is the galaxy semi-major axis. Position angle and ellipticity were held fixed. No effort was made to fit surface brightness "steps" (see Section 5.1.3) or features such as bars. Instead we focus our attention on the global photometric properties of each galaxy.

The measured optical parameters for our sample galaxies are given in Table 3. Apparent magnitudes do not include correction for Galactic extinction (although extinction values are listed in Table 1). We made no attempt to correct our derived magnitudes for internal extinction effects since these corrections are poorly know for MLSB galaxies. Based on analogies with other LSB galaxies, we believe that such corrections would be small for most of our sample due to low metallicities and dust contents (e.g., McGaugh 1994; Rönnback & Bergvall 1994; Kodaira & Yamashita 1996). We derived our inclinations based on the formula

$$\cos^2(\mathrm{i}) = \frac{(\frac{b}{a}) - q_\circ^2}{1 - q_\circ^2}$$

where $q_\circ$ for each object was assigned based on the object's Hubble type according to Heidmann *et al.* (1972) and $\frac{b}{a}$ was determined from our outermost elliptical aperture. The high frequency of optical asymmetries in extreme late-type spirals makes inclination derivations subject to more uncertainty than for HSB galaxies (see below) although the severity of this effect is difficult to quantify.

### *3.4.3. Justification of Photometry Approach*

The photometry method we describe allowed us to produce a set of useful photometric measures in an efficient manner without model-dependent assumptions. For example, azimuthal averaging of the radial light distribution may facilitate the fitting of an exponential profile to the galaxy's disk, but if features like asymmetries or off-central light concentration are ignored, valuable physical information about the galaxy is thrown away (e.g., Burstein 1979; Ohta *et al.* 1990; Odewahn 1991) and derived results can be misleading (e.g., Richter & Sancisi 1994). An examination of our galaxy images (Plates 1-7) quickly reveals that "irregularities" seem the rule rather than the exception for extreme late-type spirals. Thus it is especially important to consider this information in characterizing the optical properties of these galaxies.

To illustrate the severity of these effects, we present a full isophotal ellipse fit for three of our sample galaxies in Figure 1. It is clear that while in Panel a, the light profile of ESO 548-050 can be adequately fit by a single exponential, this characterization is deceptively simple since an examination of the galaxy image (Plate 4), clearly reveals a significant outer disk asymmetry. Panels b and c (ESO 358-015 and ESO 358-020 respectively) show cases where a single exponential does not characterize the disk's light distribution, and multiple disk components are required (neither galaxy has a discernible bulge or bar on the optical images). Here the definition of "disk scale length" as defined by a single exponential fit becomes ambiguous.

Radial surface brightness profiles of LSBs in other recent papers also show deviations from single exponentials in galaxies which do not possess bulge components (e.g., Odewahn 1991; Rönnback & Bergvall 1994). The deviations become especially striking when compared with high-quality surface brightness profiles of HSB galaxies, which are often very well fit with single exponentials (plus a bulge component; e.g., de Jong 1995, but cf. Boronson 1981).

For extreme late-type spirals, the motivation for a simple photometry approach is strengthened by practical concerns. Because images of MLSB galaxies are inherently of relatively low signal-to-noise, one must be cautious about attempting automated fitting procedures. For our data we found that the IRAF/STSDAS "ellipse" program was incapable of making suitable ellipse fits to MLSB objects in even a semi-automated manner and the program was unable to chose a unique solution, especially in the faint outer parts of the galaxy. These difficulties made automated ellipse fitting for individual galaxies unreliable if ellipse parameters are allowed to freely vary.

## 4. Sources of Photometric Uncertainty

### 4.1. The Present Dataset

The 0.9m and 1.5m telescopes with the Tek 512 and 1024 CCDs are good choices for photometry of extreme late-type spirals since both telescopes have minimal scattered light and both CCDs are cosmetically excellent with no detectable fringing. In addition, since most of our targets were field galaxies well out of the Galactic Plane, contamination from field stars was minimized. The combination of these factors allowed us to obtain flat fields, on average, to better than 2% in B and 0.4% in V with the 0.9m and 1.3% in B and 0.6% in V with the 1.5m telescope. In most frames, flatfield uncertainty was the dominant source of photometric error. See the Appendix 1 for further details on our error estimation procedure.

As a check on the accuracy of our results, we compare our B magnitudes with the photographic B magnitudes published in the ESO Catalogue (Lauberts & Valentijn 1989) for 45 of our galaxies. The results are plotted in Figure 2. An offset of $\sim +.2$ magnitudes is evident for our new results. Such an offset is consistent with that found by other workers (e.g., Rönnback & Bergvall 1994; Vader & Chaboyer 1994; Vennik *et al.* 1996) and verifies the basic integrity of our results. We note however, that the mean offset for our Night 6 data ($0.287\pm.186$ magnitudes; 7 galaxies) is larger than the mean of the other five nights ($0.047\pm.32$ magnitudes; 36 galaxies), although the scatter is large. We have no evidence that conditions were non-photometric on Night 6; however, a zero-point offset may be be present on that night. We have flagged these data in Table 3.

### 4.2. The Problems of Determining Total Magnitudes of LSB Galaxies

The conversion of a measured magnitude to a "total" magnitude for a galaxy is always fraught with uncertainties (e.g., de Vaucouleurs & Corwin 1977). Unfortunately there arises an additional set of concerns for MLSB galaxies, since a larger fraction of the galaxy's light lies in the faint outer portions of the galaxies and larger errors in the photometry from these effects are inevitable.

The outermost isophote to which we can measure in each of our galaxies depends on a variety of factors: the intrinsic properties of the disk; flatfield errors; sky subtraction errors; observation in the presence of Moonlight or twilight; intrinsic variations in sky brightness due to the Milky Way and zodiacal light; and the presence of bright field stars. We see no correlation between the color of the outer disk and the faintness of the last measured isophote as might be expected if sharper disk cutoffs are associated with younger stellar populations, while smoother edges are due to older stellar populations (Bosma 1983).

We note in our sample that edge-on galaxies can typically be traced to fainter (face-on-corrected) surface brightness levels than less inclined galaxies. However, to attempt to derive inclination-dependent magnitude corrections based on this fact would be dangerous since in a sample selected on *observed* rather than *intrinsic* surface brightness, the edge-on galaxies will always be among the intrinsically lowest (face-on corrected) surface brightness systems, hence their nature may be somewhat different. Next, since sharp radial brightness cutoffs are known to exist for some brighter galaxies at a range of surface brightness levels (e.g., Barteldrees & Dettmar 1994), it is possible that such cutoffs exist in at least some extreme late-type spirals as well. Moreover, the assumption of the symmetric, exponential nature of the disk in the outermost portions is highly questionable due to the difficulty in measuring these points in extreme late-type spirals. While it is true that for a given scale length, a galaxy with lower central surface brightness will contain a larger fraction of its light in the outer regions, pure extrapolations of fits to infinity can likewise introduce large errors for LSB disk magnitudes in the absence of empirical justification (see Tully *et al.* 1996). Moreover, definitive establishment of faint disk extensions of faint galaxies on small-field CCDs is extraordinarily difficult. Small amounts of scattered light, flatfield errors, and/or small errors in sky determinations can lead to grossly different characterizations of the outer disk profiles (e.g., Barteldrees & Dettmar 1994).

Because our survey images are only moderately deep, in order to empirically test these effects, we obtained deep V images of two of our sample galaxies (ESO 418-008 and ESO 305-009) using the CTIO Curtis Schmidt telescope in January 1995. The Curtis Schmidt has a field of view of $\sim 25'$. We obtained 6 exposures totalling 2500 seconds of integration time for ESO 418-008 and 6 exposures totalling 2400 seconds for ESO 305-009. We shifted the target to a different position on the chip between exposures. Flatfields on the Curtis Schmidt are excellent; the final frames have flatfields to better than 0.2% and 0.5% respectively.

We next compared the flux within an aperture identical to that used to photometer these galaxies in the 0.9m or 1.5m datasets. The result for ESO 418-008, which had a limiting outer

isophote of 26.6 mag arcsec$^{-2}$ in the 0.9m data, was that no additional flux was detected in the Schmidt data outside the adopted 0.9m aperture (Figure 3a). For ESO 305-009, additional flux was detected beyond the outermost 1.5m isophote (at 25.4 mag arcsec$^{-2}$) only along about one third of the periphery of the isophote (Figure 3b). This light is not very extended; its detectable extent is $\sim$0.3′ on one side of the galaxy and $\sim$0.2′ on the other. This excess light accounts for only about 1% of the total galaxy light.

While these results cannot be strictly generalized to every galaxy in the sample, they do help to show that faint disk extensions are not likely to contribute a significant amount to the total luminosity of MLSB extreme late-type spirals in most cases. We contrast this with the LSB spiral sample of de Blok *et al.* (1995), where the difference between their measured aperture magnitude and their magnitude derived from a radial light profile extrapolated to infinity ranged from 0.03 to 0.86 mags with a mean of 0.28 mags (an aperture correction of nearly 30%).

## 5. Discussion of Measured and Derived Optical Parameters

### *5.0.1. Colors and Color Gradients*

The derived aperture colors and total colors for our galaxies are presented in Table 5. The spread in total B–V (0.186–0.636) is consistent with that found in other samples of late-type spirals and irregulars with similar optical luminosities (e.g., de Vaucouleurs *et al.* 1981; Gallagher & Hunter 1986). We see no correlation of color with Hubble type (Figure 10). Our sample contains four extremely blue galaxies, (B–V<0.3) which are interesting since these may be particularly young objects (cf. Rönnback & Bergvall 1994) and because galaxies with B–V$\leq$0.4 are too blue to be accounted for by stellar population models with constant star formation rates over time scales of $\geq$10 Gyr (e.g., Charlot & Bruzual 1991; Krüger & Fritze-von Alvensleben 1994). Colors show no correlation with inclination for most of our sample (Figure 4) which further suggests that internal extinction is low. The exception is that two of the bluest galaxies in our sample actually have the *highest* derived inclinations. However, this is likely a selection effect since both galaxies have very low mean surface brightnesses and would be nearly invisible ($\bar{\mu}_V$ >26.4 mag arcsec$^{-2}$) if viewed face-on.

Figure 5 shows a plot of color versus mean surface brightness for our sample. For most of the observed range in color, the two quantities show no correlation. Similar results have been found for field samples of late-type spirals and irregulars by de Vaucouleurs *et al.* (1981) and Gallagher & Hunter (1986). Likewise, both sets of authors found the spread of color at a given Hubble type to be large as we do in our sample (see Table 5; Figure 10). The mean B–V of our full sample (0.463±.118) is not significantly different from typical colors of higher surface brightness spirals of similar Hubble types in the literature. The existence of the two very blue galaxies (B–V<0.2) with very low mean surface brightnesses ($\bar{\mu}_V$ >26 mag arsec$^{-2}$) in our sample shows that not all of the very bluest galaxies are vigorously forming stars.

de Blok *et al.* (1995) also reported that their LSB spiral sample was not significantly different in terms of B–V from HSB spirals, although they claim that B–R colors showed their LSB samples to be bluer than HSB galaxies. This is surprising since for galaxies B–V and B–R are generally correlated. For example, the sample of Rönnback & Bergvall (1994), chosen to have the bluest B–R colors in the ESO Catalogue, also showed extremely blue B–V colors (mean B–V$\sim$0.34).

From the colors in each of our three apertures, we can get an idea of the color gradient across the disk (Table 5). We find 16 cases where the galaxy becomes *redder* with increasing r. One of the cases with outward reddening is a blue compact dwarf (BCD)-like object with a very blue, bright center ((B–V)$_c$=0.39) and faint, red outer arms ((B–V)$_{out}$=0.81). As is typical with BCD systems, the mean total color of this galaxy is fairly normal (B–V=0.55) in spite of the outward reddening. Blue cores superimposed on redder, lower surface brightness backgrounds appear to be characteristic of some classes of starbursts (e.g., Hunter *et al.* 1994). In the other 15 cases we can find no obvious galaxy traits which could explain the "reverse" color gradient and it is unlikely all of the cases can be attributed to extinction or inclination effects. Objects with similar "reverse" color gradients are also found in the sample of Rönnback & Bergvall (1994). Among spirals, this trend appears to be a unique feature of certain late-type disks (e.g., Tully *et al.* 1996). Interestingly, this feature is contrary to predictions of viscous disk evolution models, which predict radial bluing of the disk (e.g., Firmani *et al.* 1996).

### *5.0.2. Surface Brightnesses*

We derived the the mean measured surface brightness for each galaxy from the formula:

$$\bar{\mu}_\lambda = \mathrm{m}_\lambda + 2.5 \log(\pi a b)$$

where $a$ and $b$ are the semi-major and semi-minor axes of the galaxy in arcminutes, respectively, and $\mathrm{m}_\lambda$ is the apparent B or V magnitude (see Table 3). We corrected this to a Galactic extinction-corrected face-on value by assuming the galaxies are optically thin and applying the formula:

$$\bar{\mu}_{\lambda,face-on} = \bar{\mu}_\lambda - 2.5 \log(\cos i) - \mathrm{A}_\lambda$$

where $i$ is the galaxy inclination and $\mathrm{A}_\lambda$ is the Galactic extinction in the appropriate waveband (see Table 4).

The mean surface brightnesses of all of our sample galaxies span the ranges (in mag arcsec$^{-2}$): $\bar{\mu}_B$=22.8–25.6 (measured); $\bar{\mu}_{B,f}$=22.9–27.0 (face-on- and Galactic extinction-corrected); $\bar{\mu}_V$=21.7–25.1 (measured); $\bar{\mu}_{V,f}$=22.4–26.8 (face-on- and Galactic extinction-corrected).

### *5.0.3. Disk Scales*

Because we did not compute azimuthally averaged light profiles for our sample galaxies, we have not derived traditional exponential scale lengths. Nonetheless, in order to provide some measure of the steepness and extent of the light profiles of the galaxies, we have derived a "mean disk scale" $\bar{\alpha}_V$ defined as: $(\bar{\mu}_{V1} - \bar{\mu}_{V2})/1.086$r, where $\bar{\mu}_{V1}$ is the mean surface brightness in V between the middle and the outermost fitted ellipses at $r_1$, $\bar{\mu}_{V2}$ is the mean V surface brightness within the innermost fitted ellipse at $r_2$, and $r = r_1 - r_2$. This measure reduces to a normal scale length in the case of a pure exponential disk. Our derived mean disk scales are given in Table 4. On average these values are smaller than the exponential scale length in other recent LSB spiral samples (e.g., McGaugh & Bothun 1994; de Blok *et al.* 1995), suggesting that our respective samples contain somewhat different (i.e., physically smaller) types of galaxies.

### *5.0.4. Correlations between Optical and HI Properties*

In order to gain further clues on the evolutionary status of our sample objects, we have made a comparison of their optical and H I properties. Figure 6 show a plot of B–V versus $\frac{\mathcal{M}_{HI}}{L_V}$, the ratio of the neutral hydrogen mass to the optical luminosity. It can be seen that the bluest galaxies in the sample all have relatively high neutral gas fractions, consistent with their status as young objects, although high $\frac{\mathcal{M}_{HI}}{L_V}$ galaxies are found over the full range in B–V color represented by our sample. The lack of blue galaxies with low $\frac{\mathcal{M}_{HI}}{L_V}$ is likely to be a real effect since originally all targets were selected from *blue*-sensitive photographic plates. The degree of scatter in the $\frac{\mathcal{M}_{HI}}{L_V}$ values among the redder sample galaxies (two orders of magnitude at B–V$\sim$0.6) is surprising since it indicates that galaxies whose colors are dominated by older stellar populations can still retain large gas fractions. These might be galaxies with large gas reservoirs in their outer disks where star formation cannot occur efficiently (e.g., Hunter & Gallagher 1986). This suggests that either the extreme late-type spirals represent a wide range in star-formation histories or that gas and star formation in extreme late-type spirals cycle in a manner different from current models.

Several of our sample galaxies have extremely high $\frac{\mathcal{M}_{HI}}{L_V}$ ratios ($\sim$3-9 in solar units); such values are reminiscent of that of the "H I Cloud" in Virgo ($\frac{\mathcal{M}_{HI}}{L_V}\sim$10), which is believed to be a very young object with an age of only roughly 1 Gyr (Salzer *et al.* 1991). This further hints that some of our sample galaxies may be extremely young. For the bulk of the sample however, the $\frac{\mathcal{M}_{HI}}{L_V}$ ratios are reminiscent of field samples of irregulars with moderately young stellar populations (e.g., Gallagher & Hunter 1986).

Further insight comes from examining $\frac{\mathcal{M}_{HI}}{L_V}$ versus mean inclination-corrected surface brightness ($\bar{\mu}_{V,i}$) (Figure 7). This plot shows that $\frac{\mathcal{M}_{HI}}{L_V}$ and surface brightness are correlated for galaxies spanning a wide range of B–V color. Thus while the highest $\frac{\mathcal{M}_{HI}}{L_V}$ galaxies in our sample may represent different evolutionary histories, or different stages in the stellar evolution in a single

family of objects, they all share the property of being some of the lowest surface brightness and structurally diffuse galaxies in our sample. Similar trends have also been found in samples of irregular galaxies (see Gallagher & Hunter 1985).

## 5.1. General Trends in the Sample

### *5.1.1. Offset Centers*

One of the features which distinguishes extreme late-type spirals from irregulars is that their optical centers can be unambiguously located through the presence of a nucleus or a nuclear region of enhanced brightness. However, in about two-thirds of our sample this light "center" is offset from the center of the outermost isophote of the galaxy by anywhere from 2-15″, indicating that intrinsic optical asymmetries occur frequently in extreme late-type spirals. Such asymmetries have been previously noted to be commonplace in other Magellanic spirals (e.g., Odewahn 1996) and extreme late-type Scd-Sdm spirals (e.g., Karachentsev *et al.* 1993).

An interesting question which remains to be explored is whether the light center is the true dynamical center of the galaxy. Matthews *et al.* (1997b) investigate how these optical asymmetries compare with the asymmetries seen in many of our sample galaxies in high-resolution, high signal-to-noise, single-dish H I spectra (see also Richter & Sancisi 1994).

### *5.1.2. Bars*

An examination of Plates 1-7 reveals that unlike in the LSB spiral sample of McGaugh *et al.* (1995), bars are not rare in our sample (see also Table 4); 37% of our sample (18 galaxies) is barred, and we have classified an addition 11 objects as transition objects (indicated *AB* in Table 4). In some cases the bars in our objects are slightly off-center, like those common in Magellanic irregular galaxies. In other cases, the bar is fairly centrally located as is typical in spirals.

We find that the occurrence of bars shows no correlation with mean disk surface brightness, contrary to the theoretical arguments of Mihos *et al.* (1997) who show, based on surface density, that LSB spirals should be very stable against the formation of bars. On the other hand, given the high frequency of bars in irregulars (e.g., de Vaucouleurs & Freeman 1972), and in Sd-Sm spirals (e.g., Feitzinger 1980; Odewahn 1996) empirically it is not surprising that they should be common among extreme late-type spirals. Such a trend was also noted by van den Bergh (1966) for DDO galaxies; bars are more frequent among small, faint DDO spirals than among larger, brighter DDO spirals. If extreme late-type spirals have very large dark halo cores compared to their disk scale lengths (as rotation curve measurements of similar galaxies suggest) then the absence of shear in the inner region could facilitate bar formation and increase a bar's longevity (Sparke 1997).

Our observation may also reflect the fact that barred objects tend to be excluded from central surface brightness-selected samples such as that of McGaugh *et al.* (1995). Dynamical studies are needed to further explore the nature of the bars in extreme late-type spirals.

### *5.1.3. Surface Brightness "Steps"*

Bosma & Freeman (1993) noted the existence of multi-component disks among LSB spirals. We see numerous examples of this phenomenon in our data (see Appendix 2; Plates 1-7). Because the greyscale images shown on the Plates are stretched to best emphasize detail in the central regions of the galaxy, the "steps" are more difficult to discern. We therefore show in Figure 8 one example, ESO 358-020, with a greyscale stretch that emphasizes the "stepped" light profile.

The existence of these surface brightness "steps" means that the surface brightness profiles of the galaxy cannot be adequately fit by a single exponential. This is best illustrated in a major axis profile plot rather than an azimuthally averaged radial profile since if the different disk components are not perfectly concentrically elliptical isophotes, radially averaging tends to smear out these gradients (see Figure 9).

The existence of surface brightness steps and general deviations from single exponential behavior of the disks, may imply a unique evolutionary status of these disks; in particular, it may be an additional signature of youth. In many giant spiral galaxies, the optical radial surface brightness profiles are close to exponential over at least 3-4 radial scale lengths (e.g., de Jong 1996). This implies that some mechanism has operated in the disks of giant galaxies to produce approximately exponential stellar density surface brightness profiles, while within the same disks the H I often shows a much slower decline in density with increasing radius. An explanation for this phenomenon by Lin & Pringle (1987) is that exponential disks result when the star formation and viscous times scales are comparable (see also Struck-Marcell 1991; Firmani *et al.* 1996). The presence of multi-component disks in the small spirals studied here then indicates that some type of break-down has occurred in this process.

One possible way to eliminate the single exponential disk might be to have a very low effective viscosity. In this case the gas would remain in a distribution determined by its initial angular momentum. Presumably this material could also form stars, albeit at low rates, and thereby possibly produce a flat outer disk. Galaxies with disk "steps" might therefore be considered to be dynamically unevolved.

The present data hint that color gradients are associated with the surface brightness "steps", although our sample is too small to establish whether these gradients are typically steeper or more abrupt than in galaxies without the "step" features. However, there is some indication that the "stepped" galaxies more often show reverse color gradients (in the sense of getting redder rather than bluer at larger radii; Section 5.0.1). Eight out of 14 "stepped" galaxies get redder with increasing r (57%), while only 8 out of 29 (28%) of the galaxies without a "stepped" surface

brightness distribution exhibit radial reddening. Perhaps then the faintest outer disk component in these galaxies may be predominantly composed of older stellar populations.

### *5.1.4. Point-like Nuclei*

Another trend which emphasizes the true spiral-like nature of our sample objects is that unresolved, point-like nuclei are relatively common. van den Bergh (1995) noted that the existence of such nuclei may be a distinguishing characteristic between spiral and irregular galaxies. Ten of our forty-nine objects in our sample have such nuclei, and five additional cases we list as possible nuclei candidates (see Appendix 2). From H$\alpha$–R-band images of most of our nucleated galaxies (Matthews & Gallagher, unpublished) we are able to ascertain that the central unresolved objects are not unfortunately placed foreground stars. Moreover, that we can even see these faint nuclei suggest the host galaxies have little or no bulge component, (as also is the case in the M33-type Sc III spirals) and that the internal extinction, even within the central regions of the galaxies, is very low (see also Matthews *et al.* 1996; Gallagher *et al.* 1997).

The existence of compact nuclei in extreme late-type spirals is surprising, since compact nuclear concentrations are thought to require strong central gravitation potentials, seemingly inconsistent with the optically diffuse centers of extreme late-type spirals. The nuclei may therefore indicate the presence of centrally concentrated dark matter. Additional spectroscopic observations and imaging with space-based resolutions are needed to establish the true nature of these nuclei. It is possible that in some cases the nuclei may be very low-luminosity AGNs like that in the nearby Sd IV spiral NGC 4395 (e.g., Filippenko & Sargent 1989; Matthews *et al.* 1996; Gallagher *et al.* 1997) or M33-like compact starburst nuclei (Kormendy & McClure 1993). An example of the latter is seen in the nearby extreme late-type Sdm IV spiral NGC 4242 (Matthews *et al.* 1996; Gallagher *et al.* 1997).

### *5.1.5. Looking for Evidence of Bulges*

It is well-know that the bulge component becomes decreasingly important among the latest spiral types. Eye inspection of our images reveals only five candidates for bulges (see Appendix 2); moreover, all but one of these (ESO 440-049) are questionable calls. Justification of true bulges in MLSB galaxies in the absence of kinematic data can be deceptively difficult, especially for nearly face-on galaxies.

In face-on systems, it is difficult to distinguish bulges from multi-component disks (see Section 5.1.3), although a circularization of the isophotes near the center is one signature of a bulge. Schombert *et al.* (1995) claim reddening in the central regions of their "dwarf spirals" as evidence for bulges, but this claim is not substantiated by their Figure 5. Moreover, the degree of reddening in the central portions of a galaxy correlates very poorly with bulge size (cf. de Jong

1995), so this is not a definitive test.

We conclude that among the extreme late-type spirals, bulges are most often very weak or non-existent although they are more common in larger LSB disks, generally of earlier Hubble type and larger scale lengths (e.g., Knezek 1993; Sprayberry *et al.* 1995b). Eventually stellar velocity dispersion measurements are needed to better explore this issue.

## 6. Are There Multiple "Families" of Faint Disk Galaxies?

The giant, very low surface brightness "Malin 1"-type objects are among the most luminous spirals known (e.g., Sprayberry *et al.* 1993). It seems clear that these Malin-1-type objects form a distinct family of LSB galaxies with a unique formation history (e.g., Hoffman *et al.* 1992) and no HSB analogues (e.g., McGaugh *et al.* 1995).

Knezek (1993) studied a sample of large LSB spirals, the majority of which would not be considered "Malin-1"-type objects, but which were nonetheless selected for their high H I masses and large scale length disks. These spirals have luminosities comparable to HSB giants, and often possess significant bulge components. Many of the LSB spirals in other recent samples (e.g., McGaugh & Bothun 1995; de Blok *et al.* 1995) could also be categorized with these objects (hereafter LSB giants). Current results suggest that the rotation curves of LSB giants are similar to radially scaled rotation curves of giant HSB galaxies (e.g., de Blok & McGaugh 1997; Salucci & Persic 1997).

How are these LSB giants related to the extreme late-type spirals we present here? At first glance, it may seem that the natural assumption is that these are all members of a single family of objects with the extreme late-type spirals being simply scaled-down versions of LSB giants. However, Wirth & Gallagher (1984) and Kormendy (1985) showed how this type of logic was misleading for lowest luminosity elliptical galaxies. They found that there exist two distinct families of small ellipticals, one similar to scaled-down versions of the giant ellipticals, and the other more structurally diffuse, and having distinct photometric properties.

At present there are several hints that there are structural differences between LSB giants and the extreme late-type spirals. One clue is the trend in the Tully-Fisher (TF) relation for extreme late-type spirals found by Matthews *et al.* (1997a). Sprayberry *et al.* (1995a) and Zwaan *et al.* (1995) both explored the TF relation for samples of LSB spirals and found them to be indistinguishable from that of HSB spirals (see also de Blok *et al.* 1996). However, Matthews *et al.* (1997a) found the extreme late-type spirals (i.e., the forty-nine galaxies presented here, plus five additional objects from Rönnback & Bergvall 1994) to fall, on average, 1.3 magnitudes below the TF relation defined by HSB galaxies. Matthews *et al.* (1997a) argue that this difference results primarily from the selection of two different galaxy populations: samples of predominantly LSB giants versus the extreme late-type spirals.

It appears then that the tendency to deviate from the TF relation (in the sense of a galaxy being underluminous for its rotational velocity) increases markedly among the smallest and least luminous MLSB disks—i.e., among the extreme late-type spirals. Further evidence for this trend comes from the fact that in our sample TF deviation is strongly correlated with mean disk scale and with optical size in the sense that the smallest galaxies are the greatest deviators and that there exist weak trends of TF deviation increasing with decreasing H I mass and with increasing $\frac{\mathcal{M}_{HI}}{L_V}$ ratios (Matthews *et al.* 1997b).

The latter trends suggest an increasing predominance of dark matter in these systems. This finding is consistent with rotation curve analyses and mass modelling which exists for a few examples of extreme late-type galaxies in the literature (e.g., Carignan 1985; Jobin & Carignan 1990; Côté *et al.* 1991; Broeils 1992; Martimbeau 1994; Rownd *et al.* 1994) and with the two TF deviators (DDO 154 and NGC 2915) discussed by Meurer *et al.* (1996). Meurer *et al.* (1996) further argue that the the BCD/late-type spiral NGC 2915 would never fall on the TF relation, even if all of its gas were converted *in situ* to stars, implying a structural uniqueness in this type of galaxy. Indeed, studies of the smallest spiral galaxies may be the key to furthering our understanding of dark matter in galaxies (e.g., Kormendy 1987; Salucci & Persic 1997).

In summary, current evidence suggests that *extreme late-type spirals are not simply scaled-down giants.* Ultimately, further detailed dynamical studies will help make to determine how different giant LSBs and extreme late-type spirals are in terms of their structure and mass distribution.

## 7. Connections with the More Distant Universe

### 7.1. Possible Links between Extreme Late-Type Spirals and Faint Blue Galaxies

About half of the galaxies in our sample have B–V$\leq$ 0.5, making them bluer than the typical lower bound to colors of giant spirals (de Jong 1995). This raises the possibility that some of the galaxies in our sample could be similar to the redshift z>0.3 "faint blue galaxies".

Whether small, extreme late-type galaxies comprise a significant fraction of the faint blue galaxies depends on the form of the luminosity function and on evolution of lower luminosity galaxies with lookback time, neither of which is currently well-determined (e.g., Marzke *et al.* 1994b; Heyl *et al.* 1997; Lin *et al.* 1997). Since we do not have a quantitative measure of the local space densities of extreme late-type spirals, we limit the present discussion to a preliminary exploration of the potential visibility of typical members of our sample at moderate redshifts. A full treatment of this topic requires evolutionary models and an evaluation of the redshift-dependent k-correction.

Consider as an example the observable properties of typical extreme late-type spirals seen at a redshift of z$\approx$0.8 in a no-evolution model. At this redshift the B-band in the rest frame shifts to

the I-band in the observer's frame. Adopting standard calibrations for B and Kron-Cousins I band (see Bessell 1993), we find that the observed and intrinsic mean surface brightness are related by

$$\mu_I(observed) \approx \mu_B(rest) + 0.7.$$

Thus a blue, intermediate surface brightness Sd-Sm galaxy from our sample, located at z=0.8, would be observed to have $\mu_I$ =23–25 mag arcsec$^2$ over a central region with a diameter of 2–5 kpc. For a low density Universe with $q_0$ =0.05 this region would have an angular sizes of about 0.3–0.8″, or well above the resolution limit of WFPC2 on the *HST*.

The isophotal luminosities of the inner, higher surface brightness central regions of some of the brighter extreme late-type spirals in the present sample have $M_B \approx$ -16 – -17, corresponding to I≈27 at z=0.8. If galaxies of this type are present at redshifts z<0.8, then they would be detectable in deep WFPC2 *HST* exposures, such as the Hubble Deep Field (Williams *et al.* 1996). Also, the small sizes and moderate-to-low surface brightnesses predicted for the cores of such galaxies are consistent with the properties of many of the faint galaxies detected in deep WFPC2 exposures by Odewahn *et al.* (1996). For comparison, analogs to common, nearby dwarf irregular galaxies will tend to be fainter when observed at moderate redshifts as a result of their generally low central surface brightnesses and lack of central light concentration.

We conclude that galaxies at z=0.8 with similar properties to present-day Sd-Sm systems would be observable with WFPC2 on *HST*. These galaxies would become increasingly detectable at lower redshifts, where they would be blue objects with moderately small angular sizes. A further and more detailed analysis that is beyond the scope of this paper is required to see if this or a related class of galaxy could be sufficiently frequent as to be a substantial component of the faint blue galaxy populations.

### 7.2. Lessons on Morphological Classification at Higher Redshifts

The large range in physical sizes and surface brightnesses of extreme late-type galaxies means that distances to these objects are difficult to estimate from optical images. Many extreme late-type galaxies that are relatively nearby can easily be mistaken for distant giant systems of earlier structural types (e.g., ESO 418-008 could be misclassified as a distant giant SBc spiral). This effect can be important, for example, on Schmidt survey plates where many galaxy images have low signal-to-noise ratios or very small angular sizes, and thus are difficult to classify. Such an effect may account in part for different shape of the local galactic luminosity functions found in different surveys, since morphological confusion adds to the difficulties in making luminosity functions in which galaxies are sorted by structural class (e.g., Bingelli *et al.* 1988; Marzke *et al.* 1994a).

The large scatter in relationships between morphology and other properties of extreme late-type galaxies may also have implications for the interpretation of populations of faint blue

galaxies. A considerable effort has gone into determining the structures of faint galaxies found in various deep exposures with the WFPC2 on the *HST* (e.g., Driver *et al.* 1995; Abraham *et al.* 1996; Odewahn *et al.* 1996). While these data are proving very valuable as a means to understand *populations* of galaxies at moderate-to-high redshifts, our results suggest they may be of limited utility in defining the *properties* of individual galaxies.

## 8. Discussion and Summary

We have presented new B and V aperture photometry for forty-nine small, late-type, moderate-to-low surface brightness field spirals. We have termed these galaxies "extreme late-type spirals". Unlike other recent photometric studies of LSB disk galaxies, this study focussed on a morphologically selected sample. Our goal was to gain insight into the nature of some of the smallest and least evolved spiral disk galaxies. These are not a new class of galaxy (see, e.g., Briggs 1997) but recent H I and optical surveys have revealed their past under-representation in Local Supercluster field samples. Data such as we present here are a necessary first step in the selection of samples for more detailed studies of individual properties, such as H I synthesis observations, optical spectroscopy, and mass modelling.

We find that extreme late-type spirals do not appear to be simply scaled-down versions of giants, but rather they are in many ways intermediate between irregulars and HSB giant spirals of similar Hubble types in terms of their global properties. In spite of their differing degrees of disk organization, both extreme late-type spirals and irregulars (as well as other MLSB spirals such as the DDO dwarfs) span similar ranges in optical luminosity, optical surface brightness, H I content, velocity width, and B–V colors (cf., Figure 10; van den Bergh 1966; de Vaucouleurs *et al.* 1981; Longmore *et al.* 1982; Gallagher & Hunter 1986).

In terms of disk structures, extreme late-type spirals are diverse; some have very faint but clearly defined arms, others have only rudimentary arms; others have very diffuse, structureless disks. This trend is obvious from Plates 1-7 and Table 4. Types of objects include spiral/irregular transition objects (e.g., ESO 430-039), compact, BCD/spiral transition objects (e.g., ESO 504-017), thick Magellanic spirals (e.g., ESO 418-009), and thin, extended Sd systems which appear to have dynamically very cold disks (e.g., ESO 482-005). For the bulk of our sample, there is no obvious link between the optical morphology and the derived optical or H I parameters (e.g., Figure 10). One of the unsolved questions is why there exists this diverse range of morphologies in an otherwise similar physical parameter space (see also Gavazzi *et al.* 1996).

H II region spectroscopy, which exists in the literature for a few analogous objects (e.g., Goad & Roberts 1981; Rönnback & Bergvall 1995), suggests that extreme late-type spirals also generally have very low metallicities, comparable to irregulars. Rotation curve analyses and mass modelling (presently available only for a few objects meeting our definition of extreme late-type spirals) suggest that like irregulars, extreme late-type spirals are often dark matter dominated, even within

the optical galaxy (e.g., Carignan 1985; Broeils 1992; Meurer *et al.* 1996). One piece of indirect evidence that this trend is widespread among extreme late-type spirals is that many of these galaxies fall below the TF relation for brighter galaxies (e.g., Matthews *et al.* 1997a), consistent with other dark matter-dominated late-type spirals and irregulars (e.g., Meurer *et al.* 1996). Other hints of dark matter domination are that these galaxies can harbor compact nuclei, the apparent longevity of bars, and that these structurally diffuse disks can maintain organized structures over a Hubble time. Together the aforementioned findings suggest that extreme late-type spirals include some of the least evolved spiral galaxies in terms of both star formation and dynamical properties.

From the derived properties of the present data we note several other interesting trends among extreme late-type spirals galaxies: (1) bars are common features [18 out of 49 galaxies in our sample are barred; 11 more objects are intermediate (*AB*) galaxies]; (2) unresolved nuclei are found in 10 of our galaxies; these may be related to low-level AGNs or M33-like compact starburst nuclei; (3) the observed range of B–V colors for our sample is similar to that of high surface brightness and moderate surface brightness samples of similar Hubble types; color is not well-correlated with surface brightness; we have four very blue objects in our sample (B–V<0.3) which may be extraordinary young objects; (4) a number of our galaxies have large H I fractions ($\frac{\mathcal{M}_{HI}}{L_V}$>3); these objects include the three bluest galaxies in our sample, but also include galaxies spanning the full range of observed B–V colors found in our sample; large $\frac{\mathcal{M}_{HI}}{L_V}$ also seems to correlate with low surface brightness over a range in color; (5) several of our sample galaxies show disk reddening with increasing radius; (6) many of our disks cannot be well fit with a single exponential disk even though they do not possess a bulge component; (7) sharp surface brightness gradients ("steps") are seen in a number of our galaxies; (8) the light centers of extreme late-type spirals are often displaced from the outermost galaxy isophote; (9) extreme late-type spirals appear to be a structurally unique family of galaxy rather than simply scale-down giant spirals; (10) higher-redshift analogues of moderate surface brightness extreme late-type spirals may comprise at least part of the faint blue galaxy populations.

We thank CTIO for their generous allocation of observing time for this project. We also thank D. M. Peterson for a critical reading of this manuscript. This research was funded by the Wide Field and Planetary Camera 2 Investigation Definition Team, which is supported at the Jet Propulsion Laboratory (JPL) via the National Aeronautics and Space Administration (NASA) under contract No. NAS7-1260 as part of a project to identify new classes of targets for WFPC2 observations.

## .1. Appendix: Error Estimation

For each galaxy we have computed an error for our derived magnitude (columns 3 & 5, Table 3) which consists of the sum in quadrature of the errors resulting from (1) shot noise, (2) read noise, (3) small-scale pixel-to-pixel variations in excess of Poisson noise, and (4) flatfield

errors. Our estimates refer to internal errors only, and do not take into account uncertainties in the photometric solution (see Table 2). An additional discussion of error analysis for galaxy CCD photometry may be found in Knezek (1993).

For some galaxies, additional uncertainty occurs if stars are present in the galaxy aperture (since they cannot be removed perfectly) and/or if the galaxy is large compared with the field-of-view of the CCD (and therefore sky flux cannot be accurately measured on the images without contamination from the galaxy light). Both of these errors are difficult to quantify, so we simply flag these cases in Table 3.

We have computed our magnitude errors from the following general formula:

$$(1) \qquad \sigma_{mag} = -2.5\ log_{10}(\frac{N_{SOURCE}}{N_{SOURCE} \pm N_{NOISE}})$$

where $N_{SOURCE}$ is the galaxy flux within the chosen aperture and $N_{NOISE}$ is the sum of all all noise sources (in electrons) within the aperture. For this work we assume that:

$$N_{NOISE} = \sqrt{\sigma^2_{POISS} + \sigma^2_{SS} + (\sigma_{FF})^2_{Sky} + (\sigma_{FF})^2_{SOURCE}}$$

We discuss each of these terms below.

### *.1.1. Poisson Noise*

In general for CCD observations,

$$\sigma_{POISS} = \sqrt{total\ electrons\ counted} = \sqrt{\frac{N_{SOURCE}}{G} + \frac{N_{SKY}}{G} + (n_{pix} \cdot RN^2)}.$$

where $N_{SOURCE}$ is the total number of electrons in the source aperture, G is the CCD gain in electrons per ADU, $N_{SKY}$ is the number of sky electrons in the aperture, measured within several "sky boxes" as described in Section 3.4.2, $n_{pix}$ is the number of pixels in the galaxy aperture, and RN is the CCD readnoise in RMS electrons per pixel.

### *.1.2. Small-Scale Pixel-to-Pixel Noise*

We measured small-scale pixel-to-pixel noise in excess of Poisson noise by computing the RMS value for all of the pixels within each individual sky box measurement ($\sigma_{BOX}$) and comparing this with the error expected from pure Poisson statistics ($\sigma_{BOX,POISS}$). Thus:

$$\sigma_{SS} = \sqrt{\sigma^2_{BOX} - \sigma^2_{BOX,POISS}}$$

where $\sigma^2_{BOX}$ is taken to be the sky box with the highest measured internal standard deviation each particular image. For most galaxies this term was negligible, unless there were many field stars or faint background galaxies in the frame.

### *.1.3. Flatfield Errors*

Because flatfield errors affect both the sky count measurement and the object count measurement, flatfield errors consist of two components. We estimated the effect of flatfield errors on our sky measures by comparing the standard deviation between the mean sky value determined from the different sky box measurements on each image with the deviation expected from pure Poisson statistics. The standard deviation between sky boxes is expressed as:

$$\sigma_{BBOX} = \sqrt{\frac{(\bar{N}_{box1}-\bar{N}_B)^2+(\bar{N}_{box2}-\bar{N}_B)^2+\ldots}{N_{tot}-1}}$$

where $N_{tot}$ is the total number of sky boxes measured, $\bar{N}_{box,n}$ is the mean counts per pixel in box n, and $\bar{N}_B = \frac{N_{box1}+N_{box2}+\ldots}{N_{tot}}$.

Assuming the distribution of pixel values within the sky box is Poisson, then each sky box pixel can be treated as an independent sky measure and we have

$$\sigma_{BOX,POISS} = \frac{\sqrt{total\ sky\ counts\ in\ sky\ box}}{n_{pix,sb}}.$$

Here, $n_{pix,sb}$ is the number of pixels within the sky box.

Over the entire galaxy aperture, the noise due to the flatfield uncertainty on the sky measurement is given by the difference, in quadrature, of the above two terms times $n_{pix}$, where $n_{pix}$ is the number of galaxy aperture pixels.

$$(\sigma_{FF})_{SKY} = [\sqrt{\sigma^2_{BBOX} - (\sigma_{BOX})^2_{POISS}}] \times n_{pix}$$

The effect of the flatfield errors on the object flux measurement can be estimated simply by scaling $(\sigma_{FF})_{SKY}$ by the ratio the source counts ($N_{SOURCE}$) to the sky counts within the galaxy aperture ($N_{SKY}$):

$$(\sigma_{FF})_{SOURCE} = (\frac{N_{SOURCE}}{N_{SKY}}) \cdot (\sigma_{FF})_{SKY}.$$

### *.1.4. Final Formula*

Finally, combining all noise terms by summing in quadrature, we arrive at the formula

$$N_{NOISE} = \{\sigma^2_{POISS} + \sigma^2_{SS} + n^2_{pix}(\sigma_{FF})^2_{SKY}(1 + (\frac{N_{SOURCE}}{N_{SKY}})^2)\}^{\frac{1}{2}}.$$

which may be used in Equation (1).

## .2. Appendix: Comments on Individual Objects

*ESO 547-020:* very flocculent structure; weak bar.

*ESO 418-008:* barred; moderately high surface brightness but very tiny spiral.

*ESO 418-009:* bright bar traced by a fairly HSB region; disk very flocculent and very symmetric.

*ESO 358-020:* point-like nucleus; barred; very twisted light distribution; HSB center with three moderately bright, compact sources embedded; 2-step disk.

*ESO 549-002:* appears to contain many H II regions; 3-step disk with irregular edges; very smooth underlying light distribution.

*ESO 359-016:* edge-on; 3-step disk; possibly barred; asymmetric light distribution.

*ESO 359-031:* barred; 2-step disk.

*SGC 0448-395:* point-like nucleus; 2-step disk; outer disk extraordinarily faint with no discernible structure.

*ESO 422-005:* =T0450-28; 2-step, diffuse disk.

*ESO 552-066:* point-like nucleus; very faint diffuse disk with a very slight central light enhancement.

*NGC 2131:* =SGC 0556-263; peculiar; very bright center with peculiarly-shaped, very diffuse disk; BCD candidate.

*ESO 425-008:* =SGC 0604-275; very faint, barred edge-on.

*AM 0605-341:* 4-step, structureless disk with a very bright bar; BCD candidate.

*ESO 497-007:* =AM 0902-253; point-like nucleus; very faint; possible arm structure visible.

*ESO 373-026:* bright bar; well-defined, fairly loosely-wound arms.

*ESO 500-032:* light from a very bright star occults part of galaxy; point-like nucleus set in brighter central region; very faint, diffuse disk with no discernible arm structure.

*ESO 377-017:* =AM 1107-363; nucleus? very structureless disk; little central light concentration.

*ESO 503-022:* nucleus? peculiar; 2-step disk; bright bar traced by a moderate surface brightness region with an extremely faint disk extension; no discernible arms.

*ESO 504-010:* barred; flared and/or warped disk.

*ESO 504-017:* =AM 1146-270; very bright center surrounded by faint, tightly-wound arms; likely a BCD or related object.

*ESO 440-039:* point-like nucleus; asymmetric light distribution; weak bar; somewhat irregular, lopsided spiral.

*ESO 440-049:* nearly face-on; dE-like companion present with $m_V$=18.0; system resembles LSB analogue of M51; likely has a bulge component; outer disk is very faint and symmetric; clearly visible arms.

*ESO 441-023:* =AM 1213-311; very faint, irregular arms; 3-step disk.

*ESO 380-025:* two-piece bar-like feature; disk appears flared; extent of disk is symmetric but light distribution is very asymmetric.

*ESO 443-080:* one-armed spiral with a well-defined single arm; has somewhat brighter nuclear region containing what appear to be two bright H II regions.

*ESO 508-034:* very bright center; possibly contains a bulge.

*ESO 445-007:* extraordinarily faint disk.

*ESO 510-026:* point-like nucleus; very faint; arms visible only in V frame; possible weak bar.

*ESO 446-053:* symmetric disk but with very asymmetric light distribution; appears to have many small H II regions.

*ESO 482-005:* near edge-on; barred; 2-step disk; outer disk very faint; possible dwarf companion.

*ESO 358-015:* point-like nucleus; very tiny 2-step disk with asymmetric light distribution; bulge?

*ESO 548-050:* nucleus? near edge-on, but arms visible; fairly HSB center; asymmetric light distribution.

*ESO 358-060:* diffuse; nearly edge-on; fairly uniform surface brightness; possibly an irregular.

*ESO 359-029:* point-like nucleus; 2-step disk; small, very smooth, diffuse disk.

*ESO 305-009:* =T0506-38; point-like nucleus; fairly diffuse disk with one faint arm; possible bulge or bar.

*ESO 487-019:* barred; arm structure superposed on smooth disk.

*ESO 488-049:* =SGC 0556-252; barred; very faint outer disk; appears to contain many small H II regions throughout disk.

*ESO 431-015:* very high Galactic extinction; little central light concentration; inclination and morphological classification uncertain.

*ESO 318-024* =AM 1055-391; peculiar "X" shape; possible merger remnant; very large bar or elongated disk structure surrounded by a diffuse outer disk or halo; inclination very uncertain.

*ESO 502-016:* barred; small, diffuse disk.

*ESO 438-005:* =T1106-28; very faint, inclined disk with faint bar; appears to contain several H II regions scattered throughout the disk.

*ESO 440-004:* nucleus? bar traced by moderately HSB region; sprawling arms nearly perpendicular to the bar; possibly a merger product.

*ESO 504-025:* possible faint nucleus; 2-step disk; very diffuse outer disk; appearance of small H II regions scattered about disk; bulge?

*ESO 505-013:* =T1203-22; point-like nucleus; well-defined, faint spiral arms; possible weak bar.

*ESO 507-065:* very tiny, moderately HSB disk with well-defined apparent outer disk cutoff; entire disk outlined in ring of what appear to be H II regions.

*ESO 443-079:* small, weak bar; very faint disk; fairly symmetric disk but with very asymmetric light distribution.

*ESO 443-083:* =T1310-22; dwarf companion present in frame.

*ESO 444-002:* peculiar "group"; Sm-like disk surrounded by several small, irregularly-shaped galaxy "fragments".

*ESO 444-033:* barred; very asymmetric light distribution.

## REFERENCES

Abraham, R. G., Tanvir, N. R., Santiago, B. X., Ellis, R. S., Glazebrook, K., & van den Bergh, S. 1996, MNRAS, 279, L47.

Arp, H.A. & Madore, B.F. 1987, *A Catalogue of Southern Peculiar Galaxies and Associations*, Vol. I, (Cambridge: Cambridge University Press).

Barteldrees, A. & Dettmar, R. -J. 1994, A&AS, 103, 475.

Bessell, M. S. 1993, in *Stellar Photometry–Current Techniques and Future Developments*, eds. C. J. Butler & I. Elliott (Cambridge: Cambridge University Press), p22.

Bingelli, B. 1993, in *A Panchromatic View of Galaxies–Their Evolutionary Puzzle*, eds. G. Hensler, Ch. Theis, J. Gallagher, (Hamburg : Astronomische Gesellschaft), p. 173.

Bingelli, B., Sandage, A., & Tammann, G. A. 1988, ARAA, 26, 509.

Boronson, T. 1981, ApJS, 46, 177.

Bosma, A. 1983, in *Internal Kinematics and Dynamics of Galaxies*, ed. E. Anthanassoula, IAU Symposium No. 100, (Dordrecht: Reidel), p. 253.

Bosma, A. & Freeman, K. C. 1993, AJ, 106, 1394.

Briggs, F. H. 1997, a preprint.

Broeils, A. H. 1992, A&A, 256, 19.

Burstein, D. 1979, ApJS, 41, 435.

Carignan, C. 1985, ApJ, 229, 59.

Charlot, S. & Bruzual, A. G. 1991, ApJ, 367, 126.

Corwin, H.G. Jr., de Vaucouleurs, A., & de Vaucouleurs, G., 1985, University of Texas Monographs, No. 4.

Côté, S. Carignan, C., & Sancisi, R. 1991, AJ, 102, 904.

de Blok, W. J. G., & McGaugh, S. S. 1997, in *Dark and Visible Matter in Galaxies*, ed. M. Persic & P. Salucci, ASP Conference Series, Vol. 117, (ASP: San Francisco), p. 39.

de Blok, W. J. G., McGaugh, S. S., & van der Hulst, J. M. 1996, MNRAS, 283, 18.

de Blok, W. J. G., van der Hulst, J. M., & Bothun, G. D. 1995, MNRAS, 274, 235.

de Jong, R. S. 1995, Ph.D. Thesis, University of Groningen, the Netherlands.

de Jong, R. S. 1996, A&A, 313, 45.

de Vaucouleurs, G. 1977, ApJS, 33, 211.

de Vaucouleurs, G. & Corwin, H. G. 1977, ApJS, 33, 219.

de Vaucouleurs, G., de Vaucouleurs, A., & Buta, R. 1981, AJ, 86, 1429.

de Vaucouleurs, G., de Vaucouleurs, A., Corwin, H. G., Buta, R. J., Paturel, G., & Fouqué, P. 1991, *The Third Reference Catalogue of Bright Galaxies* (RC3), (New York: Springer-Verlag).

de Vaucouleurs, G. & Freeman, K. C. 1972, Vistas in Astron, 14, 163.

Driver, S. P., Windhorst, R. A., & Griffiths, R. E. 1995, ApJ, 453, 448.

Feitzinger, J. V. 1980, Space Science Reviews, 27, 35.

Filippenko, A. V. & Sargent, W. L. W. 1989, ApJ, 342, L11.

Firmani, C., Hernandez, X., & Gallagher, J. 1996, A&A, 308, 403.

Fouqué, P., Bottinelli, L., Durand, N., Gouguenheim, L., & Paturel, G. 1990, A&AS, 86, 473.

Gallagher, J. S. & Hunter, D. A. 1985, AJ, 90, 1789.

Gallagher, J. S. & Hunter, D. A. 1986, AJ, 92, 557.

Gallagher, J. S., Littleton, J. E., & Matthews, L. D. 1995, AJ, 109, 2003.

Gallagher, J. S., Matthews, L. D., Krist, J., & Burrows, C. 1997, in preparation.

Gavazzi, G., Pierini, D., & Boselli, A. 1996, A&A, 312, 397.

Goad, J. W. & Roberts, M. S. 1981, ApJ 250, 79.

Heidmann, J., Heidmann, N., & de Vaucouleurs, G. 1972, Me. R. astr. Soc., 75, 85.

Heyl, J., Colless, M., Ellis, R. S., & Broadhurst, T. 1997, MNRAS, 285, 613.

Hoffman, Y., Silk, J., & Wyse, R. F. G. 1992, ApJ, 388, L13.

Hunter, D. A. & Gallagher, J. S. 1986, PASP, 98, 5.

Hunter, D. A., van Woerden, H. G., & Gallagher, J. S. 1994, ApJS, 91, 79.

Impey, C. 1993, in *Sky Surveys: Protostars to Protogalaxies*, ed. G. Neugebauer, (San Francisco: ASP).

Jobin, M. & Carignan, C. 1990, AJ, 100, 648.

Karachentsev, I. D., Karachentseva, V. E., & Parnovsky, S. L. 1993. Astron. Nachr., 314, 97.

Karachentseva, V. E., Prugniel, P., Vennik, J., Richter, G. M., Thuan, T. X., & Martin, J. M. 1996, A&AS, 117, 343.

Kent, S. M. 1984, ApJS, 56, 105.

Kent, S. M. 1985, ApJS, 59, 115.

Knapen, J. H. & van der Kruit, P. C. 1991, A&A, 248, 57.

Knezek, P. M. 1993, Ph.D. Thesis, University of Massachusetts.

Kodaira, K., Okamura, S., & Ichikawa, S. 1990, *Photometric Atlas of Northern Bright Galaxies*, (Tokyo: University of Tokyo Press).

Kodaira, K. & Yamashita, T. 1996, PASJ, 48, 581.

Kormendy, J. 1985, ApJ, 295, 73.

Kormendy, J. 1987, in *Dark Matter in the Universe*, IAU Symposium 117, (Dordrecht: Reidel), p. 139.

Kormendy, J. & McClure, R. D. 1993, AJ, 105, 1793.

Kraan-Korteweg, R. C. & Huchtmeier, W. K. 1992, A&A, 266, 150.

Krüger, H. & Fritze-v. Alvensleben, U. 1994, A&A, 284, 793.

Lauberts, A. & Valentijn, E. A. 1989, *The Surface Photometry Catalogue of the ESO-Uppsala Galaxies*, (Garching bei München: European Southern Observatory).

Lin, D. N. C. & Pringle, J. E. 1987, ApJ, 320, L87.

Lin, H., Yee, H. K. C., Carlberg, R. G., & Ellingson, E. 1997, ApJ, 475, 494.

Longmore, A. J., Hawarden, T. G., Goss, W. M., Mebold, U., & Webster, B. L. 1982, MNRAS, 200, 325.

Martimbeau, N., Carignan, C., & Roy, J.-R. 1994, AJ, 107, 543.

Marzke, R. O., Geller, M. J., Huchra, J. P., & Corwin, H. G., Jr. 1994a, AJ, 108, 437.

Marzke, R. O., Huchra, J. P., & Geller, M. J. 1994b, ApJ, 428, 434.

Matthews, L. D. & Gallagher, J. S. 1993, BAAS, 25, 845.

Matthews, L. D., Gallagher, J. S., Krist, J., Burrows, C., and the WFPC2 Science Team, 1996, BAAS, 28, 824.

Matthews, L. D., Gallagher, J. S., & van Driel, W., 1997a in *Dark and Visible Matter in Galaxies*, ed. M. Persic & P. Salucci, ASP Conference Series, Vol. 117, (ASP: San Francisco), p. 98.

Matthews, L. D., van Driel, W., & Gallagher, J. S. 1997b., in preparation.

McGaugh, S. S. 1994, ApJ, 426, 135.

McGaugh, S. S. & Bothun, G. D. 1994, AJ, 107, 530.

McGaugh, S. S., Schombert, J. M., & Bothun, G. D. 1995, AJ, 109, 2019.

Meurer, G. R., Carignan, C., Beaulieu, S. F., & Freeman, K. C. 1996, AJ, 111, 1551.

Mihos, J. C., McGaugh, S. S., de Blok, W. J. G. 1997, ApJL, in press.

Odewahn, S. C. 1991, AJ, 101, 829.

Odewahn, S. C. 1996, in *Barred Galaxies*, ASP Conference Series, Vol. 91, ed. R. Buta, D. A. Crocky, & B. G. Elmegreen, (ASP: San Francisco), p. 30.

Odewahn, S. C., Windhorst, R. A., Driver, S. P., & Keel, W. C. 1996, ApJ, 472, L13.

Ohta, K., Hamabe, M., & Wakamatsu, K. 1990, ApJ, 357, 71.

Rao, S. & Briggs, F. H. 1993, ApJ, 417, 494.

Rao, S., Turnshek, D. A., & Briggs, F. H. 1995, ApJ, 449, 448.

Richter, O. -G. & Sancisi, R. 1994, A&A, 290, L9.

Romanishin, W., Krumm, N., Salpeter, E., Knapp, G., Strom, K. M., & Strom, S. E. 1982, ApJ, 263, 94.

Rönnback, J. & Bergvall, N. 1994, A&AS, 108, 193.

Rönnback, J. & Bergvall, N. 1995, A&A, 302, 353.

Rownd, B. K., Dickey, J. M., & Helou, G. 1994, AJ, 108, 1638.

Salucci, P. & Persic, M. 1997, in *Dark and Visible Matter in Galaxies*, ed. M. Persic & P. Salucci, ASP Conference Series, Vol. 117, (ASP: San Francisco), p. 1.

Salzer, J. J., Di Serego Alighieri, S., Matteucci, F., Giovanelli, R., & Haynes, M. P. 1991, AJ, 101, 1258.

Schombert, J. M., Bothun, G. D., Schneider, S. E., & McGaugh, S. S. 1992, AJ, 103, 1107.

Schombert, J. M., Pildis, R. A., Eder, J. A., & Oemler, A. Jr. 1995, AJ, 110, 2067.

Sparke, L. S. 1997, private communication.

Sprayberry, D., Impey, C. D., Irwin, M. J., McMahon, R. G., & Borne, G.D. 1993, ApJ, 417, 114.

Sprayberry, D., Bernstein, G. M., Impey, C. D., & Bothun, G. D. 1995a, ApJ, 438, 72.

Sprayberry, D., Impey, C. D., Bothun, G. D., & Irwin, M. J. 1995b, AJ, 109, 558.

Struck-Marcell, C. 1991, ApJ, 368, 348.

Thuan, T. X. & Seitzer, P. O. 1979, ApJ, 231, 680.

Tully, R. B. 1988, *Nearby Galaxies Catalog*, (Cambridge: Cambridge University Press).

Tully, R. B. & Fouqué, P. 1985, ApJS, 58, 67.

Tully, R. B., Verheijen, M. A. W., Pierce, M. J., Huang, J.-S., & Wainscoat, R. J. 1996, AJ, 122, 2471.

Vader, J. P. & Chaboyer, B. 1994, AJ, 108, 1209.

van den Bergh, S. 1966, AJ, 71, 922.

van den Bergh, S. 1995, AJ, 110, 613.

van der Hulst, J. M., Skillman, E. D., Smith, T. R., Bothun, G. D., McGaugh, S. S., & de Blok, W. J. G. 1993, AJ, 106, 548.

van der Kruit, P. C. 1987, A&A, 173, 59.

van Zee, L., Haynes, M. P., Salzer, J. J., & Broeils, A. H. 1997, AJ, 113, 1618.

Vennik, J., Richter, G. M., Thänert, W., & Biering, C. 1996, Astron. Nachr., 317, 289.

Williams, R .E., Blacker, B., Dickinson, M., Dixon, W. V. D., Ferguson, H. C., Fruchter, A. S., Giavalisco, M., Gilliland, R. L., Heyer, I., Katanis, R., Zolt, L., Lucas, R. A., McElroy, D. B., Petro, L., Postman, M., Adorf, H.-M., & Hook, R. N. 1996, AJ, 112, 1335.

Wirth, A. & Gallagher, J. S., III, 1984, ApJ, 282, 85.

Zwaan, M. A., van der Hulst, J. M., de Blok, W. J. G., & McGaugh, S. S. 1995, MNRAS, 273, L35.

Fig. 1.— Azimuthally averaged V-band surface brightness profiles (corrected for inclination and Galactic extinction) versus radius, in arcseconds, for three of our extreme late-type spirals. These light profiles are based on full ellipse fits to the images. The solid lines are exponential fits to the inner portions of the disk.

Fig. 2.— Our new B-band CCD magnitudes versus the photographic B magnitudes published for a number of our sample galaxies in the ESO Catalogue. The solid line is x=y.

Fig. 3.— V-band images of two of our extreme late-type spirals taken with the Curtis Schmidt telescope. Panel a shows a 2500 second exposure of ESO 418-008 ($\sim 1.4' \times 1.4'$) with the outermost fitted ellipse from our fits to the 0.9m data overplotted. No excess light is visible outside of this ellipse in the Schmidt data. Panel b shows ESO 305-009 ($\sim 2.6' \times 2.6'$) with the outermost fitted ellipse from our fits to the 1.5m data overplotted. A small amount of additional light is visible beyond this ellipse in the northeast and southwest corners of the image. This light totals less than $\sim$1% of the total measured flux of the galaxy.

Fig. 4.— B–V color versus inclination for our extreme late-type spiral sample.

Fig. 5.— B–V color versus mean V surface brightness (corrected for Galactic extinction and inclination) for our extreme late-type spiral sample.

Fig. 6.— B–V color versus the logarithm of the ratio of the H I mass to the V-band luminosity (corrected for Galactic extinction) in solar units.

Fig. 7.— Mean V surface brightness (corrected for Galactic extinction and inclination) versus the logarithm of the ratio of the H I mass to the V luminosity (corrected for Galactic extinction) in solar units.

Fig. 8.— Greyscale image of ESO 358-020, stretched to emphasize the abrupt change in surface brightness of the disk or surface brightness "step".

Fig. 9.— Major axis cut of ESO 358-020, plotted as pixel number versus the logarithm of the counts per pixel. A three pixel-wide strip along the galaxy major axis was sampled. The dotted line emphasizes the sharp change in slope in surface brightness (i.e. the surface brightness "step") which occurs in the light profile of this galaxy. The delineation of this feature becomes smeared out when the light profile is azimuthally averaged (see Figure 2b).

Fig. 10.— Fundamental galaxy parameters (logarithm of the H I mass; B - V; and absolute V magnitude) versus Hubble Type (as assigned from the present data set; see Table 4) for our extreme late-type spiral sample.

Fig. 11.— Plates: V-band images of our extreme late-type spiral galaxies. Plates 1–3 show our 0.9m data and Plates 4–7 are the 1.5m data. Each object frame was individually scaled to best emphasize the galaxy's morphology in the central regions.

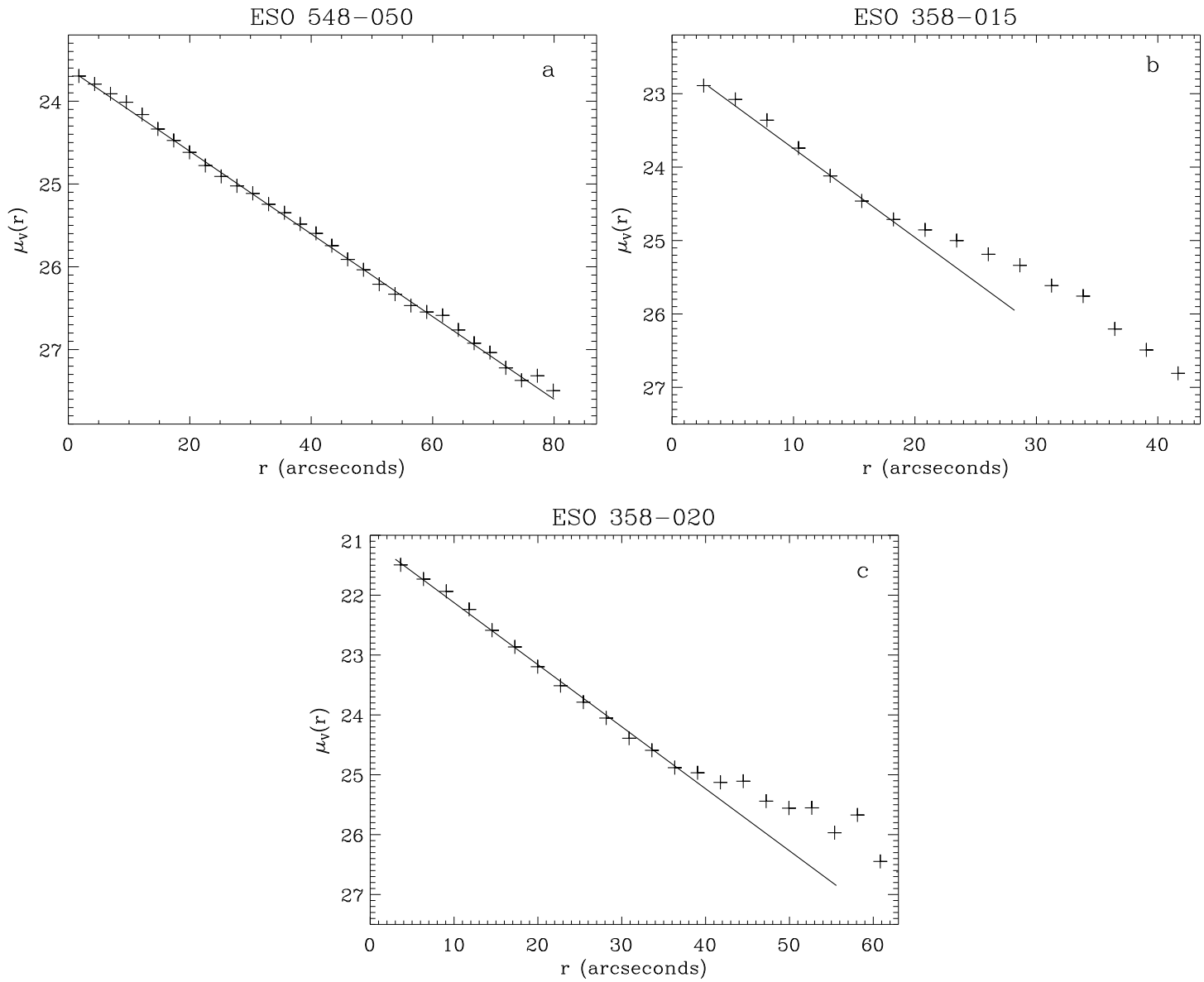
ESO 548−050
a
$\mu_V(r)$
r (arcseconds)
ESO 358−015
b
$\mu_V(r)$
r (arcseconds)
ESO 358−020
c
$\mu_V(r)$
r (arcseconds)

TABLE 1. Program Objects

| Galaxy Name (1) | ESO Type (2) | $\alpha$ (1950.0) (3) | $\delta$ (1950.0) (4) | $V_r$ (5) | $\mathcal{M}_{\mathcal{HI}}$ (6) | D (7) | $m_{B,ESO}$ (8) | $A_B$ (9) |
|---|---|---|---|---|---|---|---|---|
| ESO547-020 | 9.0 | 03 10 40 | -18 06 54 | 1994 | 9.08 | 26.6 | 15.38 | 0.06 |
| ESO418-008 | 8.0 | 03 29 28 | -30 22 54 | 1194 | 8.65 | 15.0 | 13.90 | 0.00 |
| ESO418-009 | 10.0 | 03 29 54 | -31 30 18 | 956 | 8.09 | 11.8 | 14.07 | 0.00 |
| ESO482-005 | 8.0 | 03 30 52 | -24 18 06 | 1915 | 8.90 | 25.0 | 15.46 | 0.01 |
| ESO358-015 | 9.0 | 03 31 10 | -34 58 30 | 1390 | 8.08 | 17.4 | 15.34 | 0.00 |
| ESO358-020 | 10.0 | 03 32 58 | -32 48 18 | 1789 | 7.90 | 22.8 | 14.58 | 0.0 |
| ESO548-050 | 8.0 | 03 33 25 | -21 27 24 | 1803 | 9.00 | 23.6 | 14.67 | 0.03 |
| ESO549-002 | 10.0 | 03 40 43 | -19 10 48 | 1108 | 7.90 | 14.43 | 14.78 | 0.13 |
| ESO358-060 | 10.0 | 03 43 18 | -35 43 30 | 805 | 8.31 | 9.40 | 15.86 | 0.00 |
| ESO359-016 | 10.0 | 04 02 34 | -36 19 00 | 1408 | 8.58 | 17.3 | 15.00 | 0.00 |
| ESO359-029 | 10.0 | 04 10 56 | -33 07 42 | 873 | 7.84 | 10.2 | 14.77 | 0.00 |
| ESO359-031 | 8.0 | 04 11 17 | -34 33 12 | 1486 | 8.30 | 18.6 | 14.56 | 0.00 |
| SGC0448-395 | ... | 04 48 30 | -39 52 49 | 2250 | 8.93 | 27.9 | ... | 0.00 |
| ESO422-005 | 8.0 | 04 50 07 | -28 40 30 | 1460 | 8.94 | 16.9 | 14.88 | 0.00 |
| ESO552-066 | 10.0 | 05 03 02 | -18 27 30 | 1684 | 8.47 | 21.3 | 16.25 | 0.09 |
| ESO305-009 | 8.0 | 05 06 26 | -38 22 30 | 1022 | 9.30 | 11.1 | 13.08 | 0.06 |
| ESO487-019 | 8.0 | 05 29 45 | -23 10 48 | 1829 | 8.82 | 22.7 | 13.84 | 0.08 |
| ESO488-049 | 8.0 | 05 56 38 | -25 25 06 | 1766 | 9.20 | 21.5 | 15.01 | 0.08 |
| NGC2131 | 10.0 | 05 56 47 | -26 39 18 | 1659 | 9.01 | 20.0 | 14.59 | 0.00 |
| ESO425-008 | 9.0 | 06 04 38 | -27 52 18 | 1459 | 8.45 | 17.2 | 16.57 | 0.00 |
| AM0605-341 | ... | 06 05 31 | -34 11 49 | 772 | 8.00 | 7.8 | ... | 0.04 |
| ESO431-015 | 5.0 | 08 30 59 | -30 13 30 | 1133 | 8.53 | 11.7 | ... | 0.80 |
| ESO497-007 | 10.0 | 09 02 59 | -25 34 30 | 2570 | 8.86 | 30.8 | 16.45 | 0.72 |
| ESO373-026 | 4.0 | 09 44 39 | -33 22 24. | 2465 | 9.50 | 29.0 | ... | 0.70 |
| ESO500-032 | 8.0 | 10 20 30 | -24 05 06 | 2371 | 8.68 | 28.0 | 14.76 | 0.28 |
| ESO318-024 | 9.0 | 10 55 33 | -39 10 18 | 999 | 8.80 | 9.30 | 14.00 | 0.34 |
| ESO502-016 | 9.0 | 11 02 48 | -26 21 18 | 1512 | 8.33 | 16.4 | 14.72 | 0.25 |
| ESO438-005 | 8.0 | 11 06 33 | -28 06 00 | 1499 | 9.43 | 21.4 | 14.87 | 0.22 |
| ESO377-017 | 10.0 | 11 07 56 | -36 36 18 | 2388 | 9.30 | 27.9 | 16.93 | 0.32 |
| ESO503-022 | 10.0 | 11 31 00 | -26 40 18 | 1875 | 8.56 | 21.3 | 14.81 | 0.22 |
| ESO504-010 | 8.7 | 11 40 32 | -23 09 18 | 1932 | 8.62 | 22.2 | 15.54 | 0.15 |
| ESO440-004 | 8.0 | 11 43 11 | -28 05 24 | 1845 | 9.27 | 20.9 | 14.21 | 0.38 |
| ESO504-017 | 3.0 | 11 46 15 | -27 06 00 | 1856 | 9.21 | 21.1 | 13.99 | 0.44 |
| ESO504-025 | 9.0 | 11 51 18 | -27 04 18 | 1637 | 8.74 | 18.2 | 14.34 | 0.34 |
| ESO440-039 | 10.0 | 11 59 24 | -29 57 30 | 2060 | 8.60 | 23.7 | 15.76 | 0.22 |
| ESO440-049 | 7.0 | 12 02 59 | -31 08 42 | 2264 | 8.91 | 26.4 | 13.77 | 0.34 |
| ESO505-013 | 8.0 | 12 03 33 | -22 34 18 | 1718 | 9.89 | 25.7 | 13.04 | 0.22 |
| ESO441-023 | 9.2 | 12 13 01 | -31 17 12 | 2395 | 8.71 | 28.2 | 16.05 | 0.32 |
| ESO380-025 | 7.0 | 12 21 56 | -35 07 54 | 2788 | 9.10 | 33.4 | 14.76 | 0.21 |
| ESO507-065 | 10.0 | 12 58 23 | -25 49 24 | 2563 | 9.10 | 30.8 | 15.93 | 0.40 |
| ESO443-079 | 9.5 | 13 07 38 | -27 42 18 | 2123 | 9.05 | 24.9 | 15.30 | 0.27 |
| ESO443-080 | 8.5 | 13 08 25 | -27 44 36 | 2113 | 9.37 | 24.8 | 14.14 | 0.27 |
| ESO443-083 | 5.3 | 13 10 09 | -32 25 24 | 2382 | 9.72 | 33.3 | 13.31 | 0.19 |
| ESO444-002 | 8.0 | 13 14 00 | -27 37 24 | 1642 | 8.94 | 18.6 | 15.02 | 0.19 |
| ESO508-034 | 9.0 | 13 14 13 | -25 04 24 | 1910 | 9.21 | 22.2 | 14.84 | 0.32 |
| ESO444-033 | 9.0 | 13 23 16 | -31 52 12 | 2423 | 8.98 | 28.9 | 14.94 | 0.16 |
| ESO445-007 | 10.0 | 13 37 30 | -31 26 54 | 1657 | 8.65 | 18.8 | 16.65 | 0.11 |
| ESO510-026 | 9.0 | 13 54 46 | -25 32 54 | 2366 | 9.30 | 28.6 | 15.49 | 0.30 |

TABLE 1. (continued)

| Galaxy Name (1) | ESO Type (2) | $\alpha$ (1950.0) (3) | $\delta$ (1950.0) (4) | $V_r$ (5) | $\mathcal{M}_{\mathcal{HI}}$ (6) | D (7) | $m_{B,ESO}$ (8) | $A_B$ (9) |
|---|---|---|---|---|---|---|---|---|
| ESO446-053 | 10.0 | 14 18 22 | -29 02 06 | 1398 | 8.56 | 15.7 | 14.67 | 0.31 |

References for Table 1.

(1) Fouqué *et al.* 1990; (2) Gallagher *et al.* 1995; (3) Tully 1988; (4) Kraan-Korteweg & Huchtmeier 1992.

Notes to Table 1.

Explanation of columns: (1) galaxy name; (2) ESO Catalogue morphological classification (3) & (4) right ascension and declination, epoch 1950.0; (5) heliocentric radial velocity in km $s^{-1}$, taken from references 1, 2, 3, or 4; (6) logarithm of HI mass in solar units, based on HI fluxes from refs. 1, 2, 3, & 4, distances in column 7, and $H_o$=75 km $s^{-1}$ $Mpc^{-1}$; (7) distance in Mpc based on radial velocity in column 5, after correction for motion with respect to the Local Group, and adopting a linear Hubble law with $H_o$=75 km $s^{-1}$ $Mpc^{-1}$; (8) apparent blue magnitude from the ESO Catalogue; (9) B-band Galactic extinction from the ESO Catalogue.

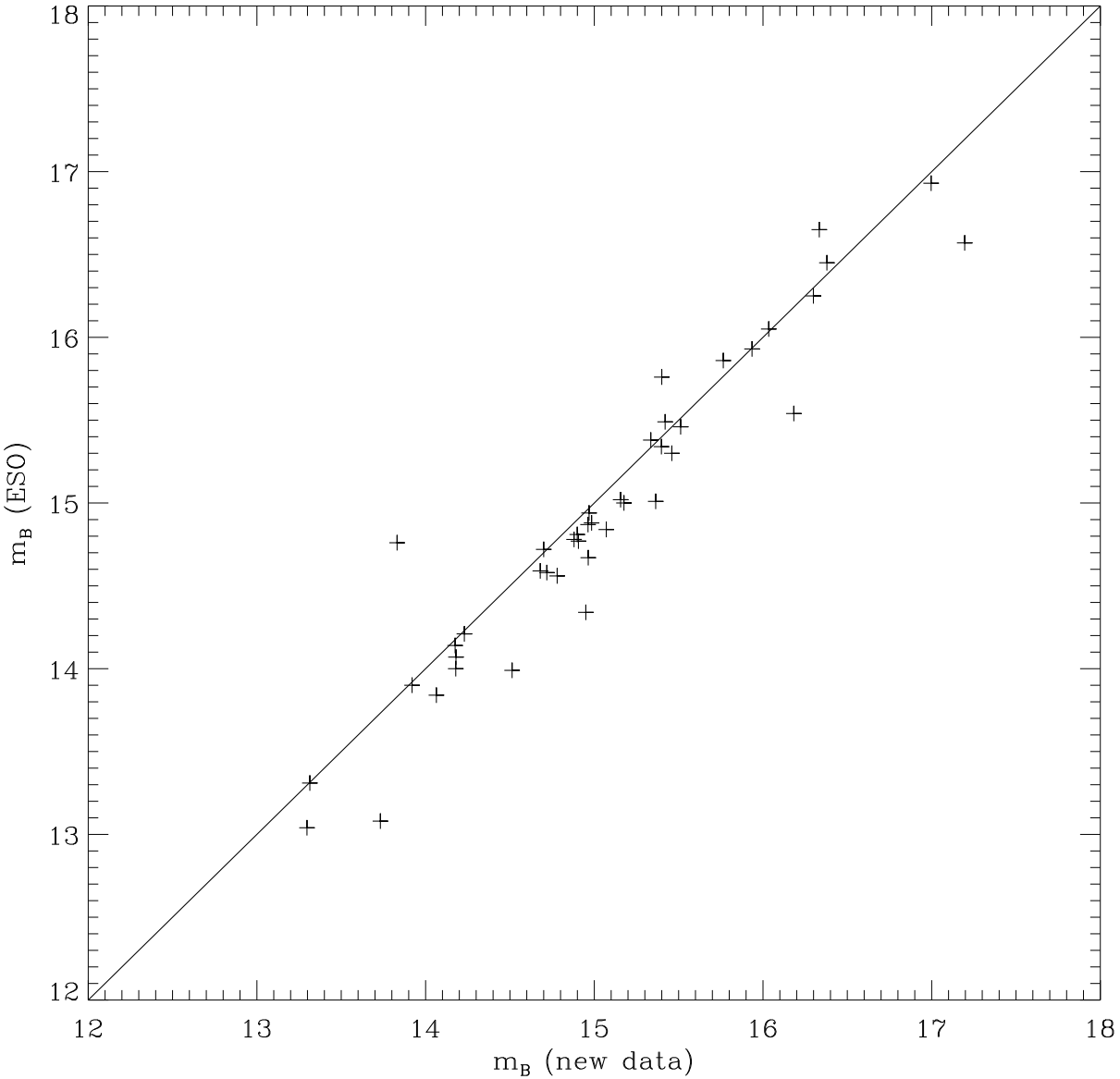
18
17
16
15
14
13
12
12
13
14
15
16
17
18
$m_B$ (ESO)
$m_B$ (new data)

TABLE 2. Photometric Transformations

| Telescope | CCD | RN ($e^-$) | Gain ($e^-$/ADU) | Transformation Equation |
|---|---|---|---|---|
| 0.9m (nights 1-5) | Tek 512 | 7.7 | 4.28 | B-V = -0.454 - 0.103($X_B$ - 1) + (b-v) + 0.138(b-v)<br>V = -4.34 + v - 0.263($X_V$ - 1) |
| 1.5m (nights 6-8) | Tek 1024 | 3.77 | 2.97 | B-V = -0.773 - (0.177($X_B$ - 1)) + (b-v) + 0.256((b-v) - 0.177($X_B$ - 1))<br>V = -2.64 - ($X_V$×0.498) + v - 0.037((b-v) - 0.177($X_V$ - 1)) |

Notes to Table 2.

Explanation of symbols: v = instrumental V-band magnitude; b = instrumental B-band magnitude; (b-v) = instrumental B - V color; $X_V$ = airmass of V-band observation; $X_B$ = airmass of B-band observation.

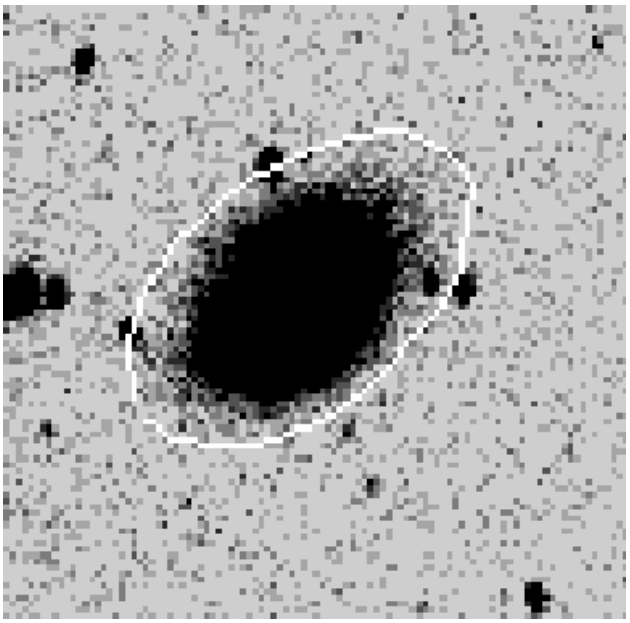

Fig. 3a.—

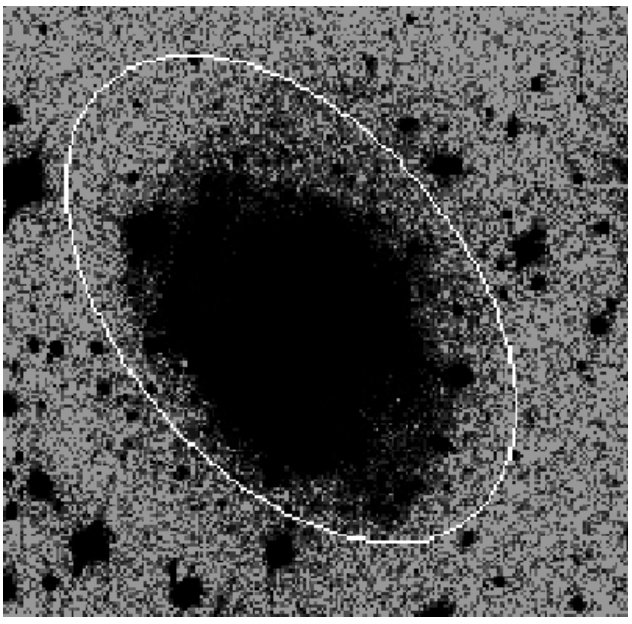

Fig. 3b.—

TABLE 3. Model-Free Photometric Parameters

| Galaxy Name (1) | $m_{B,25}$ (2) | $m_B$ (3) | $m_{V,25}$ (4) | $m_V$ (5) | Size (′) (6) | $\mu_{B,sky}$ (7) | $\mu_{V,sky}$ (8) | $\bar{\mu}_B$ (9) | $\bar{\mu}_V$ (10) | $SB_{V,outer}$ (11) | a (  |
|---|---|---|---|---|---|---|---|---|---|---|---|
| **0.9m Data:** | | | | | | | | | | | |
| ESO547-020 | 15.9 | 15.34±.031 | 14.8 | 14.86±.031 | 1.85 | 22.3 | 21.1 | 24.99 | 24.52 | 26.0 | 1 |
| ESO418-008 | 13.9 | 13.92±.015 | 13.5 | 13.51±.010 | 1.91 | 22.4 | 21.5 | 23.36 | 22.96 | 26.6 | 1 |
| ESO418-009 | 14.3 | 14.18±.025 | 13.7 | 13.67±.013 | 1.68 | 22.4 | 21.6 | 23.75 | 23.25 | 26.0 | 1 |
| ESO358-020 | 15.0 | 14.72±.026 | 14.2 | 14.13±.024 | 1.93 | 22.7 | 21.9 | 24.53 | 23.94 | 26.4 | 1 |
| ESO549-002 | 15.1 | $14.88\pm^{.190}_{.230}$ | 14.4 | 14.26±.020 | 2.06 | 22.6 | 21.8 | 24.77 | 24.14 | 25.8 | 1 |
| ESO359-016 | 15.2 | $15.18\pm^{.136}_{.156}$ | 14.7 | 14.64±.016 | 2.02 | 22.7 | 21.9 | 23.91 | 23.37 | 27.3 | 3 |
| ESO359-031 | 14.9 | 14.78±.032 | 14.3 | 14.22±.013 | 1.37 | 22.0 | 21.0 | 23.98 | 23.42 | 25.6 | 1 |
| SGC0448-39 | 17.2 | $16.86\pm^{.240}_{.310}$ | 16.5 | 16.38±.024 | 1.05 | 22.5 | 21.7 | 24.78 | 24.30 | 26.6 | 2 |
| ESO422-005 | 15.1 | 14.98±.170 | 14.8 | 14.59±.019 | 1.70 | 22.6 | 21.8 | 24.46 | 24.06 | 26.1 | 1 |
| ESO552-066 | 16.3 | 16.30±.072 | 15.8 | 15.79±.095 | 1.42 | 21.9 | 21.0 | 25.13 | 24.62 | 25.6 | 1 |
| NGC2131 | 14.7 | 14.68±.024 | 14.2 | 14.20±.003 | 1.13 | 22.0 | 21.0 | 22.82 | 22.34 | 25.3 | |
| ESO425-008 | 17.4 | 17.20±.084 | 17.4 | 17.06±.110 | 1.20 | 21.9 | 21.1 | 24.72 | 24.58 | 27.3 | |
| AM0605-341 | 14.6 | 14.54±.007 | 14.1 | 14.09±.012 | 1.27 | 22.6 | 21.7 | 23.57 | 23.12 | 26.1 | 1 |
| ESO497-007 | 16.8 | $16.38\pm^{.352}_{.531}$ | 16.2 | 15.90±.034 | 1.48 | 22.4 | 21.6 | 25.62 | 25.14 | 26.0 | 1 |
| ESO373-026 | ··· | ··· | 13.1 | 13.15±.021 | 2.22 | ··· | 20.9 | ··· | 23.52 | 24.5 | |
| ESO500-032 | ··· | $13.83\pm^{.660}_{1.94}$ | ··· | $13.24\pm^{.653}_{1.85}$ | 1.76 | 21.4 | 20.9 | 23.45 | 22.86 | 23.3 | 1 |
| ESO377-017 | 17.3 | 17.0±.056 | 16.4 | 16.33±.040 | 1.56 | 22.2 | 21.3 | 25.20 | 24.54 | 27.1 | 3 |
| ESO503-022 | 14.9 | 14.90±.021 | 14.3 | 14.31±.004 | 1.53 | 21.0 | 20.5 | 23.70 | 23.11 | 25.6 | |
| ESO504-010 | 16.4 | 16.18±.040 | 15.8 | 15.6603 | 1.44 | 22.4 | 21.6 | 24.61 | 24.09 | 26.6 | 2 |
| ESO504-017 | 14.5 | 14.51±.070 | 14.0 | 13.96±.011 | 1.10 | 22.4 | 21.6 | 23.18 | 22.63 | 25.9 | 1 |
| ESO440-039 | 15.6 | 15.40±.041 | 15.0 | 14.80±.010 | 1.70 | 22.3 | 21.6 | 24.75 | 24.15 | 26.5 | 1 |
| ESO440-049 | ··· | ··· | 13.9 | 13.89±.034 | 2.22 | ··· | 20.4 | ··· | 24.08 | 25.8 | 1 |
| ESO441-023 | 16.3 | 16.03±.024 | 15.5 | 15.45±.035 | 1.26 | 22.0 | 21.3 | 25.11 | 24.53 | 25.5 | 1 |
| ESO380-025 | ··· | ··· | 14.1 | 14.15±.009 | 1.63 | ··· | 20.3 | ··· | 22.33 | 25.4 | |
| ESO443-080 | 14.1 | 14.18±.033 | 13.8 | 13.78±.005 | 1.89 | 21.2 | 20.7 | 23.60 | 23.20 | 25.0 | 1 |
| ESO508-034 | 15.0 | 15.07±.044 | 14.4 | 14.49±.022 | 1.53 | 21.2 | 20.7 | 23.76 | 23.18 | 25.6 | 2 |
| ESO445-007 | 16.3 | 16.33±.041 | 16.1 | 16.12±.021 | 1.14 | 21.3 | 20.4 | 24.26 | 24.05 | 26.1 | 2 |
| ESO510-026 | 15.7 | $15.42\pm^{.133}_{.151}$ | 14.9 | $14.82\pm^{.136}_{.156}$ | 1.68 | 21.3 | 20.4 | 24.93 | 24.33 | 25.7 | 1 |
| ESO446-053 | ··· | ··· | 13.5 | 13.58±.009 | 1.23 | ··· | 19.1 | ··· | 21.67 | 24.3 | 2 |
| **1.5m Data:** | | | | | | | | | | | |

TABLE 3. (continued)

| Galaxy Name (1) | $m_{B,25}$ (2) | $m_B$ (3) | $m_{V,25}$ (4) | $m_V$ (5) | Size (′) (6) | $\mu_{B,sky}$ (7) | $\mu_{V,sky}$ (8) | $\bar{\mu}_B$ (9) | $\bar{\mu}_V$ (10) | $SB_{V,outer}$ (11) |
|---|---|---|---|---|---|---|---|---|---|---|
| ESO482-005 | 15.7 | 15.51±.051* | 15.0 | 15.02±.023* | 2.60 | 22.5 | 21.8 | 24.36 | 23.87 | 25.8 |
| ESO358-015 | 15.6 | 15.40±.071* | 15.0 | 14.86±.018* | 1.53 | 22.5 | 21.7 | 24.54 | 24.00 | 26.0 |
| ESO548-050 | 15.0 | 14.96±.016* | 14.5 | 14.42±.008* | 2.92 | 22.4 | 21.6 | 24.28 | 23.73 | 25.4 |
| ESO358-060 | 15.8 | 15.76±.023 | 15.8 | 15.58±.034 | 2.24 | 22.2 | 21.5 | 24.28 | 24.10 | 25.6 |
| ESO359-029 | 14.9 | 14.91±.035 | 14.3 | 14.29±.024 | 1.92 | 22.3 | 21.5 | 24.33 | 23.71 | 25.0 |
| ESO305-009 | 14.5 | $13.73\pm^{.14}_{.17}$* | 13.2 | 13.11±.053* | 4.63 | 22.6 | 21.8 | 25.15 | 24.53 | 25.4 |
| ESO487-019 | 14.1 | 14.06±.016* | 13.5 | 13.41±.010* | 2.05 | 22.4 | 21.7 | 23.70 | 23.05 | 25.2 |
| ESO488-049 | 15.7 | 15.36±.034* | 15.0 | 14.83±.016* | 2.02 | 22.4 | 21.8 | 24.68 | 24.15 | 25.5 |
| ESO431-015 | ... | ... | 16.4 | 16.38±.051 | 1.40 | ... | 21.7 | ... | 24.0 | 24.6 |
| ESO318-024 | 14.4 | 14.18±.025* | 13.7 | 13.54±.010* | 3.06 | 22.2 | 21.6 | 24.85 | 24.21 | 25.6 |
| ESO502-016 | 14.8 | 14.70±.032* | 14.2 | 14.12±.018* | 2.46 | 22.1 | 21.3 | 24.29 | 23.71 | 26.1 |
| ESO438-005 | 15.0 | 14.96±.029* | 14.6 | 14.52±.048* | 3.40 | 22.1 | 21.4 | 24.50 | 24.05 | 25.3 |
| ESO440-004 | 14.4 | $14.23\pm^{.235}_{.300}$ | 14.1 | $13.90\pm^{.115}_{.129}$ | 3.73 | 22.1 | 21.3 | 24.78 | 24.45 | 25.6 |
| ESO504-025 | 15.0 | 14.95±.056 | 14.6 | 14.34±.021 | 2.42 | 22.2 | 21.4 | 25.22 | 24.61 | 26.0 |
| ESO505-013 | 13.2 | 13.30±.082* | 12.8 | 12.82±.075* | 2.96 | 22.0 | 21.3 | 24.23 | 23.75 | 24.9 |
| ESO507-065 | 15.9 | 15.94±.073 | 15.5 | 15.51±.029 | 1.26 | 22.1 | 21.3 | 24.01 | 23.58 | 24.2 |
| ESO443-079 | 15.7 | 15.46±.019 | 15.1 | 15.01±.033 | 2.18 | 22.1 | 21.4 | 24.51 | 24.06 | 26.0 |
| ESO443-083 | 13.2 | 13.31±.006 | 12.8 | 12.76±.003 | 3.70 | 21.9 | 21.1 | 23.09 | 22.54 | 24.8 |
| ESO444-002 | 15.4 | 15.16±.012 | 14.8 | 14.75±.012 | 1.45 | 22.2 | 21.4 | 24.41 | 24.01 | 25.5 |
| ESO444-033 | 15.0 | 14.97±.032 | 14.6 | 14.54±.007 | 2.03 | 22.2 | 21.5 | 23.79 | 23.35 | 25.4 |

Notes to Table 3.

Explanation of columns: (1) galaxy name; (2) estimated apparent B magnitude within the 25 mag arcsec$^{-2}$ isophote; (3) measured apparent blue apert
V magnitude within the 25 mag arcsec$^{-2}$ isophote; (5) measured apparent V aperture magnitude; (6) diameter in arcminutes at the outermost measured
(7) & (8) mean B and V sky surface brightnesses for image, in mag arcsec$^{-2}$; (9) & (10) mean measured B and V surface brightnesses (no extinction or
brightness in magnitudes arcsec$^{-2}$ of the last measured isophote; (12) axial ratio; (13) position angle, in degrees; (14) inclination, in degrees (see Text); (

*asterisks denote cases where there may be a zero point uncertainty in both B and V of up to 0.24 magnitudes

[a]many field stars present in galaxy aperture; photometric uncertainty likely to be larger than the formally quoted error

[b]galaxy large compared with field of view; additional photometric uncertainty may result from poor sky background determination

[c]no B data obtained

[d]very bright star occults much of galaxy; large photometric uncertainty

[e]possible stellar contamination in galaxy aperture

[f]peculiarly shaped galaxy isophotes; inclination uncertain

[g]photometry includes main galaxy only, not the possible companions (see Plates)

[h]high Galactic extinction (see Table 1)

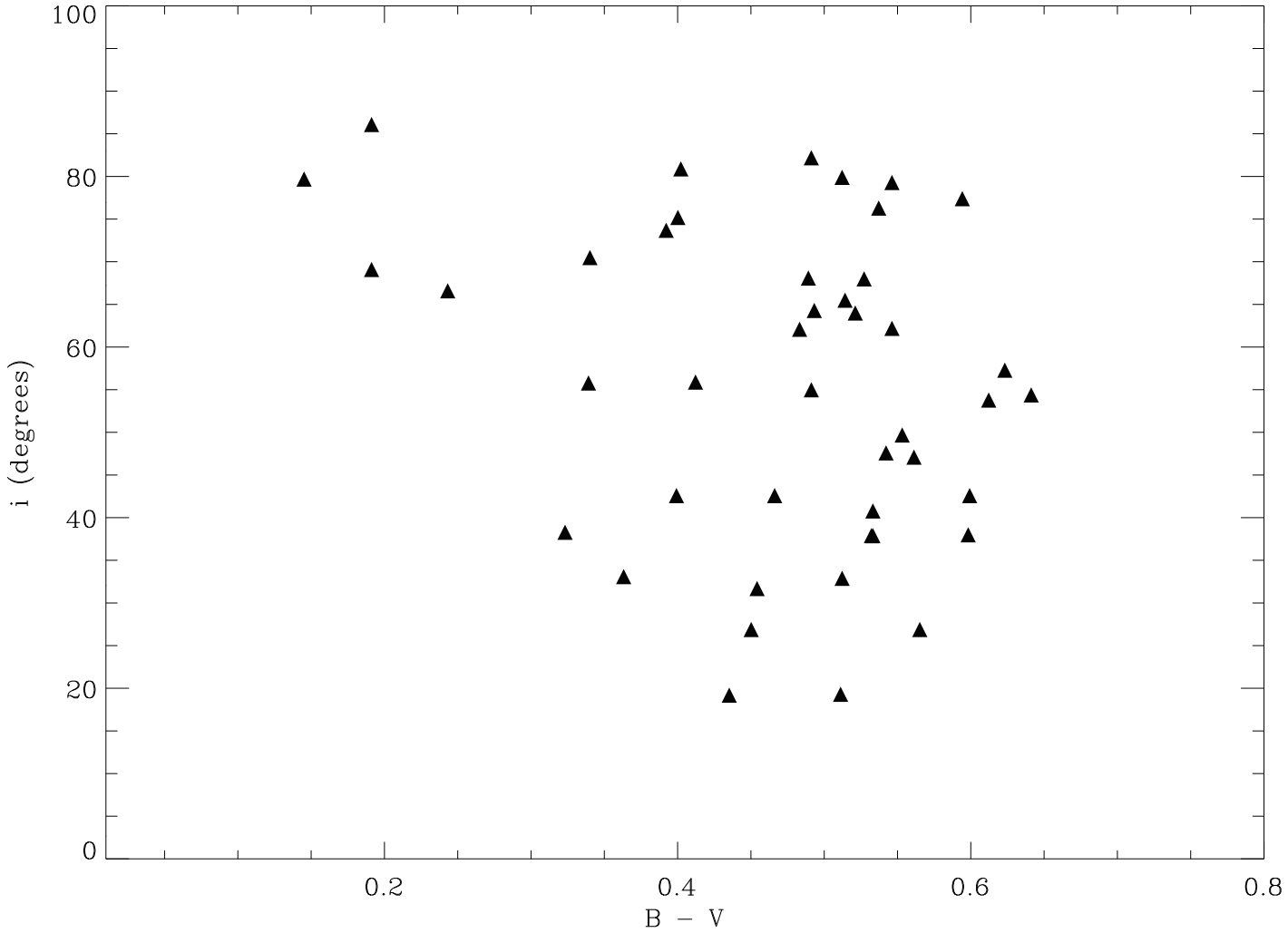
100
80
60
40
20
0
i (degrees)
0.2
0.4
0.6
0.8
B − V

TABLE 4. Derived Optical Parameters

| Galaxy Name (1) | Class (2) | $M_B$ (3) | $M_V$ (4) | $A_{outer}$ (5) | $\bar{\alpha}_V$ (6) | $\log\frac{\mathcal{M}_{HI}}{L_V}$ (7) | $\bar{\mu}_{B,face-on}$ (8) | $\bar{\mu}_{V,face-on}$ (9) |
|---|---|---|---|---|---|---|---|---|
| **0.9m Data:** | | | | | | | | |
| ESO547-020 | SBdm | -16.8 | -17.3 | 14.5 | 3.02 | 0.24 | 25.2 | 24.8 |
| ESO418-008 | SBd | -17.0 | -17.4 | 8.33 | 0.87 | -0.21 | 24.0 | 23.6 |
| ESO418-009 | SBdm | -16.2 | -16.7 | 5.75 | 0.69 | -0.50 | 23.9 | 23.4 |
| ESO358-020 | SBdm | -17.1 | -17.7 | 12.8 | 1.42 | -1.08 | 24.8 | 24.2 |
| ESO549-002 | SABdm | -16.1 | -16.6 | 8.8 | 2.39 | -0.66 | 25.0 | 24.4 |
| ESO359-016 | SABd | -16.0 | -16.6 | 10.2 | 1.22 | 0.038 | 25.4 | 24.9 |
| ESO359-031 | SBd | -16.6 | -17.1 | 7.42 | 1.06 | -0.47 | 24.1 | 23.5 |
| SGC0448-39 | SABm | -15.4 | -15.8 | 8.55 | 1.45 | 0.67 | 25.6 | 25.2 |
| ESO422-005 | Sdm | -16.1 | -16.5 | 8.38 | 1.20 | 0.40 | 24.8 | 24.4 |
| ESO552-066 | Sm | -15.4 | -15.9 | 8.91 | 3.02 | 0.19 | 25.6 | 25.1 |
| NGC2131 | BCD? | -16.8 | -17.3 | 6.56 | 0.87 | 0.17 | 23.6 | 23.1 |
| ESO425-008 | SBm: | -14.0 | -14.1 | 6.01 | 1.55 | 0.88 | 26.5 | 26.4 |
| AM0605-341 | SBdm | -15.0 | -15.4 | 2.89 | 0.88 | -0.08 | 23.6 | 23.2 |
| ESO497-007 | SABm | -16.8 | -16.9 | 15.0 | 4.66 | 0.18 | 25.2 | 24.8 |
| ESO373-026 | SBc | ··· | -19.9 | 21.1 | 3.92 | -0.38 | ··· | 23.0 |
| ESO500-032 | Scd: | -18.7 | -19.2 | 15.1 | 8.18 | -0.92 | 23.4 | 22.9 |
| ESO377-017 | Sm | -15.6 | -16.1 | 13.3 | 4.59 | 0.94 | 26.5 | 25.9 |
| ESO503-022 | SBm pec | -17.0 | -17.5 | 9.86 | 1.45 | -0.36 | 24.3 | 23.7 |
| ESO504-010 | SBdm | -15.7 | -16.2 | 9.52 | 1.48 | 0.23 | 25.5 | 25.0 |
| ESO504-017 | Scd/BCD | -17.5 | -18.0 | 7.25 | 0.61 | 0.095 | 22.9 | 22.4 |
| ESO440-039 | SBm | -16.7 | -17.2 | 12.2 | 1.89 | -0.21 | 25.0 | 24.4 |
| ESO440-049 | Sc | ··· | -18.5 | 18.1 | 2.34 | -0.39 | ··· | 24.0 |
| ESO441-023 | SABm | -16.5 | -17.0 | 10.9 | 2.82 | -0.023 | 24.8 | 24.3 |
| ESO380-025 | SBdm | ··· | -18.7 | 16.4 | 2.62 | -0.28 | ··· | 23.8 |
| ESO443-080 | Scd | -18.1 | -18.4 | 14.3 | 2.50 | 0.094 | 23.9 | 23.6 |
| ESO508-034 | S pec | -17.0 | -17.5 | 10.4 | 1.49 | 0.30 | 24.4 | 23.8 |
| ESO445-007 | SABm: | -15.1 | -15.3 | 6.38 | 1.65 | 0.60 | 25.2 | 25.0 |
| ESO510-026 | SBcd | -17.2 | -17.7 | 14.7 | 2.49 | 0.31 | 24.9 | 24.3 |
| ESO446-053 | SABdm | ··· | -17.6 | 5.92 | 0.97 | -0.41 | ··· | 22.4 |
| **1.5m Data:** | | | | | | | | |
| ESO482-005 | SBd | -16.5 | -17.0 | 19.0 | 2.51 | 0.19 | 26.4 | 25.9 |
| ESO358-015 | Sdm | -15.8 | -16.3 | 7.72 | 1.10 | -0.37 | 25.0 | 24.4 |
| ESO548-050 | SABcd | -16.9 | -17.5 | 20.2 | 3.13 | 0.096 | 26.0 | 25.4 |
| ESO358-060 | Sm | -14.1 | -14.3 | 6.13 | 1.19 | 0.68 | 27.0 | 26.8 |
| ESO359-029 | Sd | -15.1 | -15.8 | 5.71 | 1.0 | -0.38 | 25.0 | 24.4 |
| ESO305-009 | SABc | -16.6 | -17.2 | 15.1 | 2.93 | 0.52 | 25.6 | 25.0 |
| ESO487-019 | SBd | -17.8 | -18.4 | 13.7 | 1.74 | -0.47 | 24.2 | 23.5 |
| ESO488-049 | SBcd | -16.4 | -16.9 | 12.8 | 1.78 | 0.52 | 25.5 | 24.9 |
| ESO431-015 | Sm: | ··· | -14.6 | 5.46 | 1.48 | 0.78 | ··· | 25.7 |
| ESO318-024 | S pec | -16.0 | -16.6 | 8.76 | 1.32 | 0.26 | 24.9 | 24.4 |
| ESO502-016 | SBd | -16.6 | -17.1 | 12.2 | 1.38 | -0.44 | 25.1 | 24.5 |
| ESO438-005 | SBd | -16.9 | -17.3 | 21.9 | 4.58 | 0.59 | 26.2 | 25.8 |
| ESO440-004 | SBcd | -17.8 | -18.0 | 24.2 | 3.65 | 0.16 | 25.4 | 25.1 |
| ESO504-025 | Sd | -16.7 | -17.2 | 13.6 | 2.05 | -0.063 | 25.2 | 24.6 |
| ESO505-013 | SABc | -19.0 | -19.4 | 23.0 | 4.16 | 0.21 | 24.1 | 23.6 |
| ESO507-065 | Sm pec | -16.9 | -17.2 | 12.0 | 3.27 | 0.29 | 24.8 | 24.4 |
| ESO443-079 | SABd | -16.8 | -17.2 | 16.5 | 2.19 | 0.26 | 25.6 | 25.2 |

TABLE 4. (continued)

| Galaxy Name (1) | Class (2) | $M_B$ (3) | $M_V$ (4) | $A_{outer}$ (5) | $\bar{\alpha}_V$ (6) | $\log\frac{\mathcal{M}_{HI}}{L_V}$ (7) | $\bar{\mu}_{B,face-on}$ (8) | $\bar{\mu}_{V,face-on}$ (9) |
|---|---|---|---|---|---|---|---|---|
| ESO443-083 | Scd | -19.5 | -20.0 | 37.0 | 4.47 | -0.19 | 24.7 | 24.2 |
| ESO444-002 | Sm pec | -16.4 | -16.7 | 8.08 | 1.25 | 0.33 | 24.4 | 24.0 |
| ESO444-033 | SBdm | -17.5 | -17.9 | 17.5 | 2.21 | -0.092 | 25.0 | 24.6 |

Notes to Table 4.

Explanation of columns: (1) galaxy name; (2) updated Hubble classification based on new data; (3) absolute B magnitude, corrected for Galactic extinction using the extinctions and distances quoted in Table 1; (4) absolute V magnitude, corrected for Galactic extinction; (5) diameter, in kiloparsecs, at outermost measured isophote and corrected for Galactic extinction according to the RC3 (de Vaucouleurs *et al.* 1991); (6) mean disk scale in V-band in kiloparsecs (see Text); (7) logarithm of HI mass over V-band luminosity, in solar units; (8) Galactic extinction-corrected, mean B-band surface brightness in mags arcsec$^{-2}$ within the last measured galaxy isophote, corrected to a face-on value (see Text); (9) Galactic extinction-corrected, mean V-band surface brightness in mags arcsec$^{-2}$ within the last measured galaxy isophote, corrected to a face-on value.

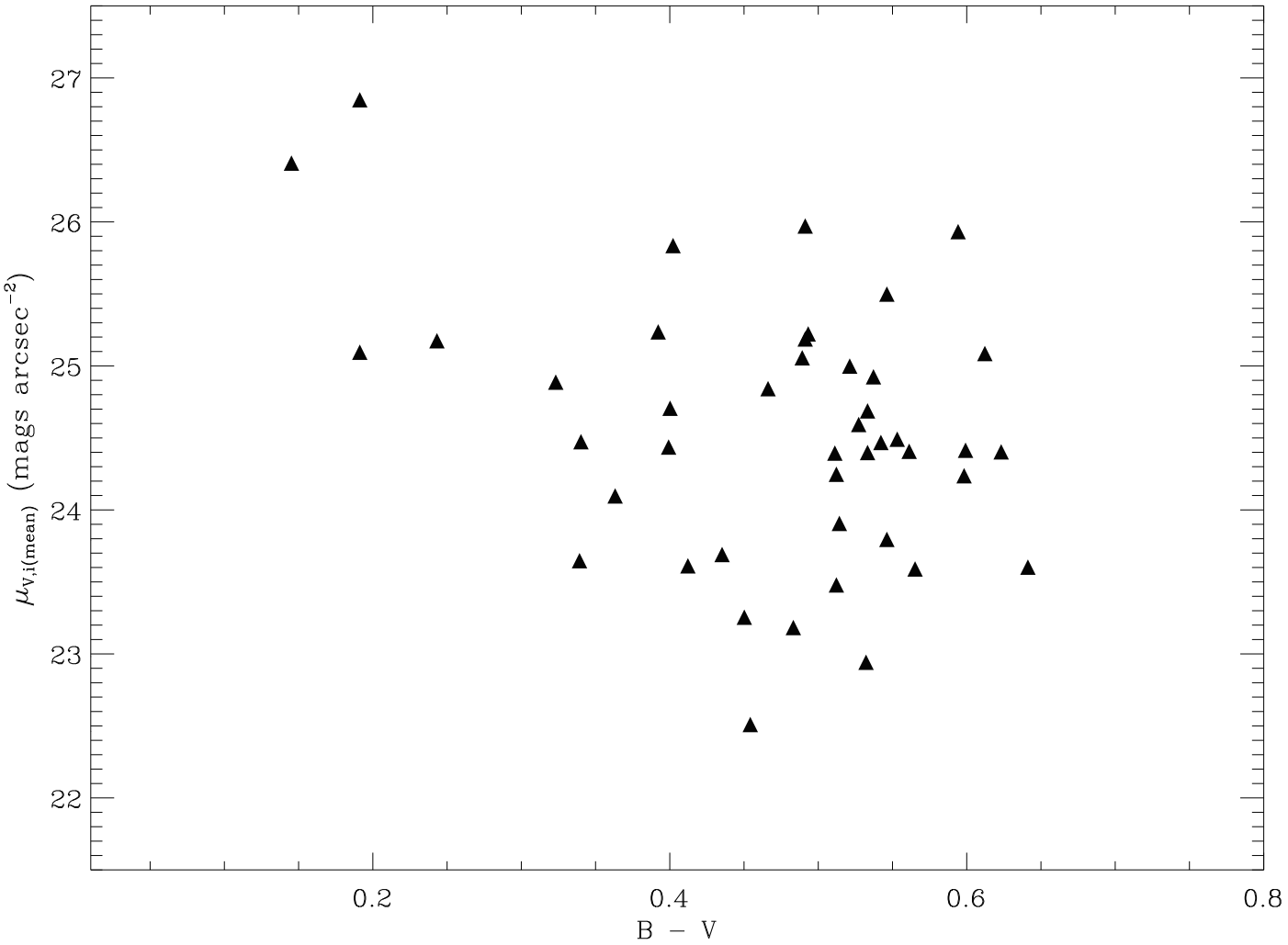
27
26
25
24
23
22
$\mu_{V,i(mean)}$ (mags arcsec$^{-2}$)
0.2
0.4
0.6
0.8
B − V

TABLE 5. B – V Colors

| Galaxy | (B – V)$_{TOT}$ | (B – V)$_{annuli}$ | | |
|---|---|---|---|---|
| | | *nuclear* | *middle disk* | *outer disk* |
| (1) | (2) | (3) | (4) | (5) |
| **0.9m Data:** | | | | |
| ESO547-020 | 0.461 | 0.548 | 0.580 | 0.336 |
| ESO418-008 | 0.407 | 0.476 | 0.348 | 0.376 |
| ESO418-009 | 0.507 | 0.553 | 0.498 | 0.454 |
| ESO358-020 | 0.593 | 0.537 | 0.673 | 0.634 |
| ESO549-002 | 0.594 | 0.508 | 0.541 | 0.762 |
| ESO359-016 | 0.532 | 0.450 | 0.504 | 0.755 |
| ESO359-031 | 0.560 | 0.700 | 0.562 | 0.413 |
| SGC0448-39 | 0.488 | 0.569 | 0.508 | 0.407 |
| ESO422-005 | 0.394 | 0.363 | 0.390 | 0.438 |
| ESO552-066 | 0.486 | 0.521 | 0.476 | 0.478 |
| NGC2131 | 0.478 | ... | ... | ... |
| ESO425-008 | 0.140 | 0.433 | 0.317 | -0.06 |
| AM0605-341 | 0.445 | 0.380 | 0.503 | 0.572 |
| ESO497-007 | 0.318 | 0.466 | 0.331 | 0.225 |
| ESO373-026 | ... | ... | ... | ... |
| ESO500-032 | 0.527 | 0.583 | 0.494 | 0.528 |
| ESO377-017 | 0.589 | 0.516 | 0.552 | 0.665 |
| ESO503-022 | 0.541 | 0.527 | 0.494 | 0.616 |
| ESO504-010 | 0.484 | 0.505 | 0.435 | 0.514 |
| ESO504-017 | 0.449 | 0.392 | 0.460 | 0.813 |
| ESO440-039 | 0.548 | 0.513 | 0.500 | 0.659 |
| ESO440-049 | ... | ... | ... | ... |
| ESO441-023 | 0.506 | 0.370 | 0.505 | 0.573 |
| ESO380-025 | ... | ... | ... | ... |
| ESO443-080 | 0.334 | 0.309 | 0.419 | 0.289 |
| ESO508-034 | 0.509 | 0.607 | 0.475 | 0.435 |
| ESO445-007 | 0.186 | 0.543 | -0.138 | 0.316 |
| ESO510-026 | 0.528 | 0.622 | 0.505 | 0.467 |
| ESO446-053 | ... | ... | ... | ... |
| **1.5m Data:** | | | | |
| ESO482-005 | 0.486 | 0.656 | 0.514 | 0.260 |
| ESO358-015 | 0.537 | 0.556 | 0.562 | 0.487 |
| ESO548-050 | 0.541 | 0.556 | 0.505 | 0.567 |
| ESO358-060 | 0.186 | 0.250 | 0.250 | 0.094 |
| ESO359-029 | 0.618 | 0.630 | 0.611 | 0.615 |
| ESO305-009 | 0.607 | 0.604 | 0.587 | 0.622 |
| ESO487-019 | 0.636 | 0.658 | 0.588 | 0.676 |
| ESO488-049 | 0.516 | 0.618 | 0.372 | 0.548 |
| ESO431-015 | ... | ... | ... | ... |
| ESO318-024 | 0.556 | 0.466 | 0.521 | 0.699 |
| ESO502-016 | 0.522 | 0.540 | 0.476 | 0.565 |
| ESO438-005 | 0.397 | 0.481 | 0.416 | 0.331 |
| ESO440-004 | 0.238 | 0.436 | 0.317 | 0.010 |
| ESO504-025 | 0.528 | 0.593 | 0.513 | 0.479 |
| ESO505-013 | 0.430 | 0.578 | 0.408 | 0.347 |
| ESO507-065 | 0.335 | 0.441 | 0.393 | 0.252 |
| ESO443-079 | 0.387 | 0.436 | 0.391 | 0.316 |

TABLE 5. (continued)

| Galaxy | $(B-V)_{TOT}$ | | $(B-V)_{annuli}$ | |
|---|---|---|---|---|
| | | *nuclear* | *middle disk* | *outer disk* |
| (1) | (2) | (3) | (4) | (5) |
| ESO443-083 | 0.507 | 0.566 | 0.446 | 0.510 |
| ESO444-002 | 0.358 | 0.478 | 0.430 | 0.176 |
| ESO444-033 | 0.395 | 0.473 | 0.357 | 0.334 |

Notes to Table 5.

Ellipses denote cases where no B data were obtained. Explanation of columns: (1) B–V color of the entire galaxy within the last measured isophote, corrected for Galactic extinction; (2), (3), & (4) differential B–V colors, corrected for Galactic extinction, in each of the three measured annuli (see Section 3.4.2).

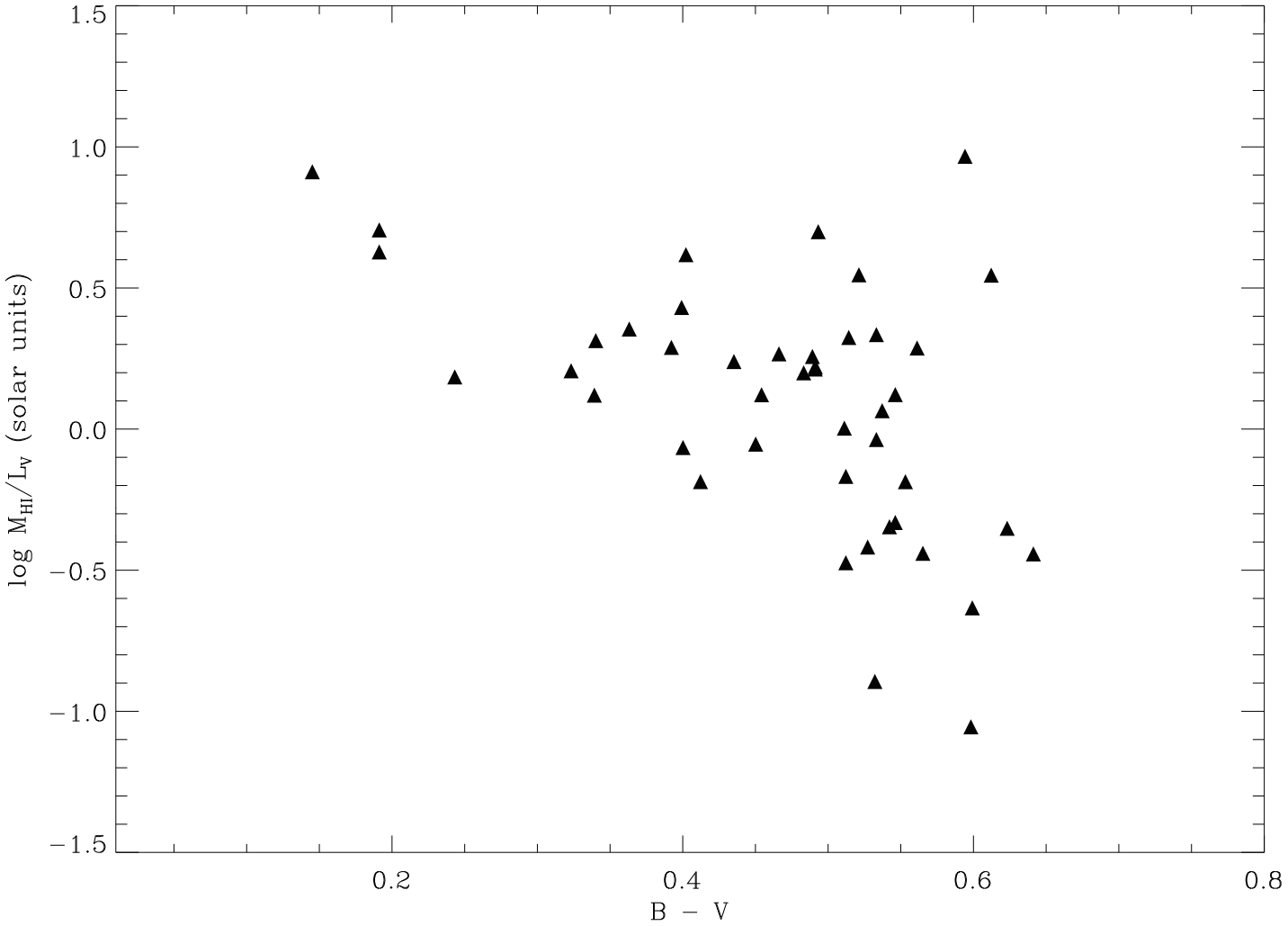
1.5
1.0
0.5
0.0
−0.5
−1.0
−1.5
log $M_{HI}/L_V$ (solar units)
0.2
0.4
0.6
0.8
B − V

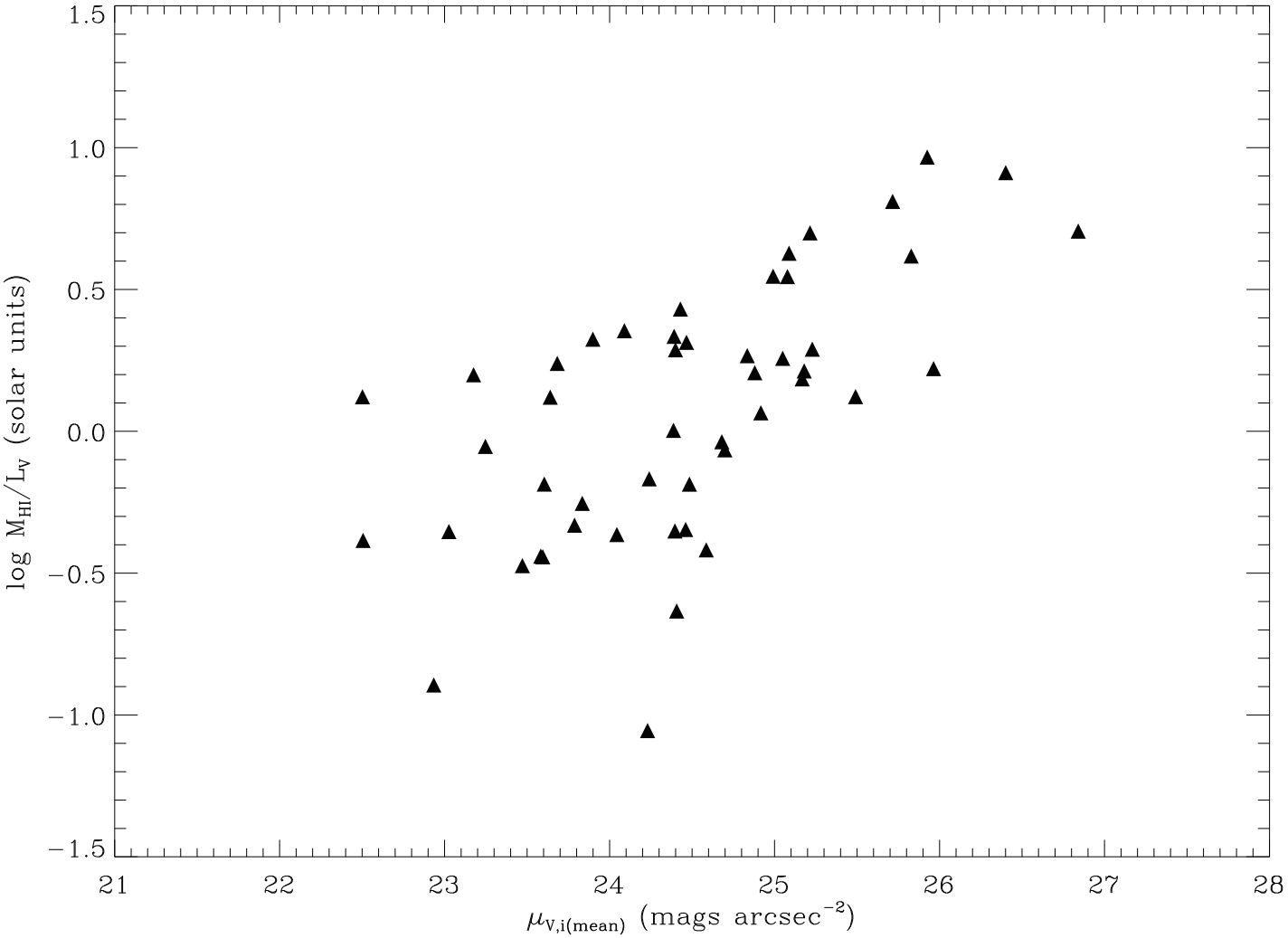
1.5
1.0
0.5
0.0
−0.5
−1.0
−1.5
log $M_{HI}/L_V$ (solar units)
21
22
23
24
25
26
27
28
$\mu_{V,i(mean)}$ (mags arcsec$^{-2}$)

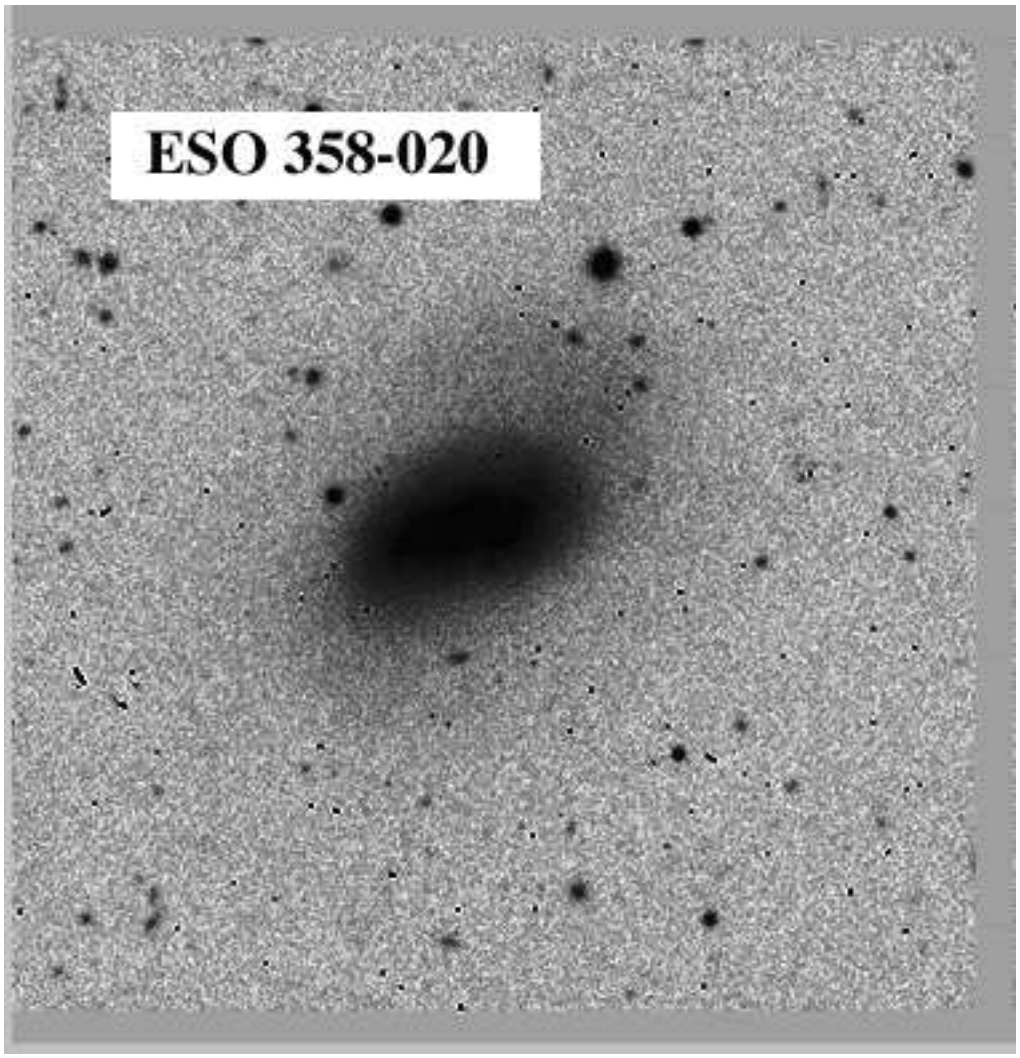
ESO 358-020

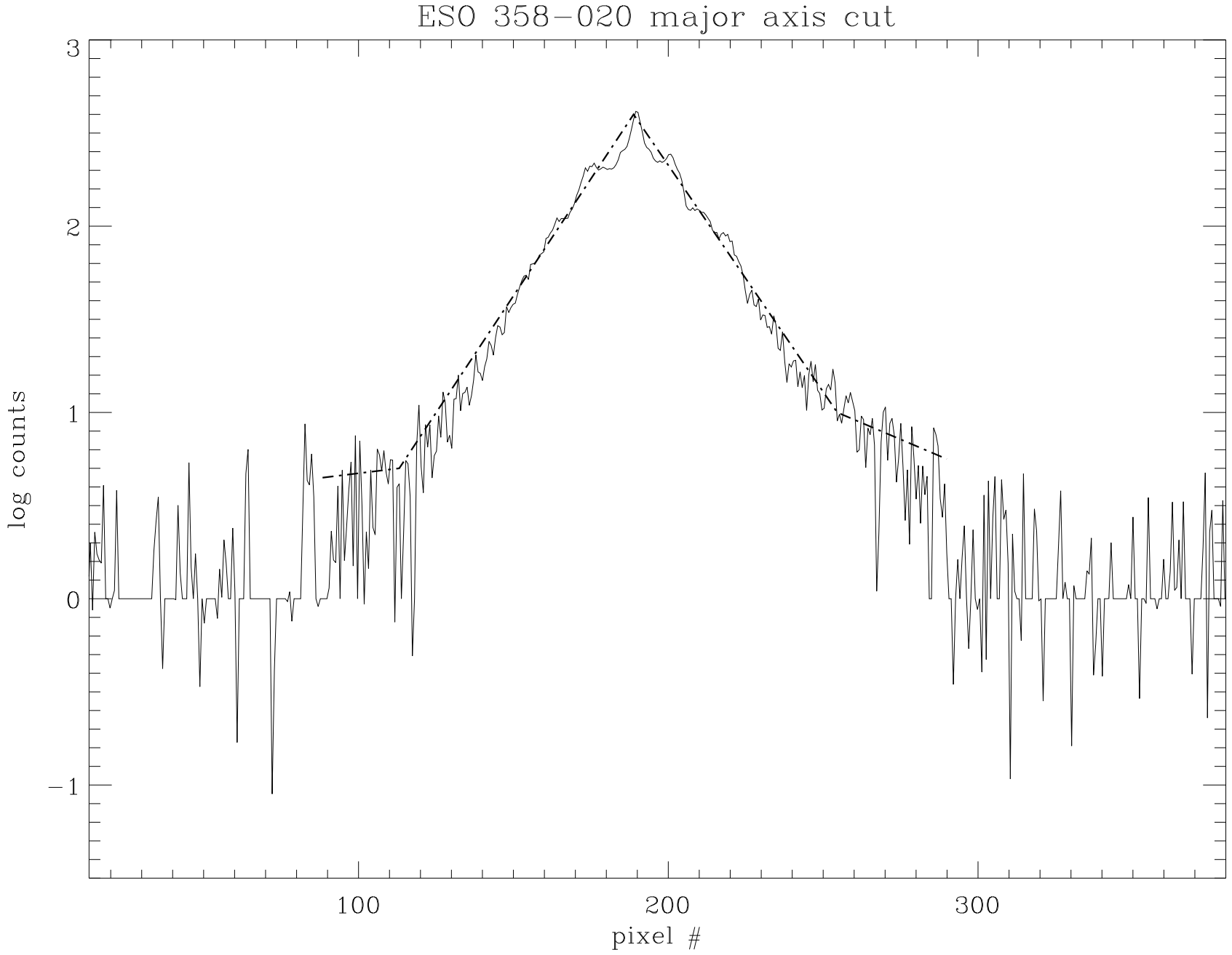
ESO 358−020 major axis cut
log counts
3
2
1
0
−1
100
200
300
pixel #

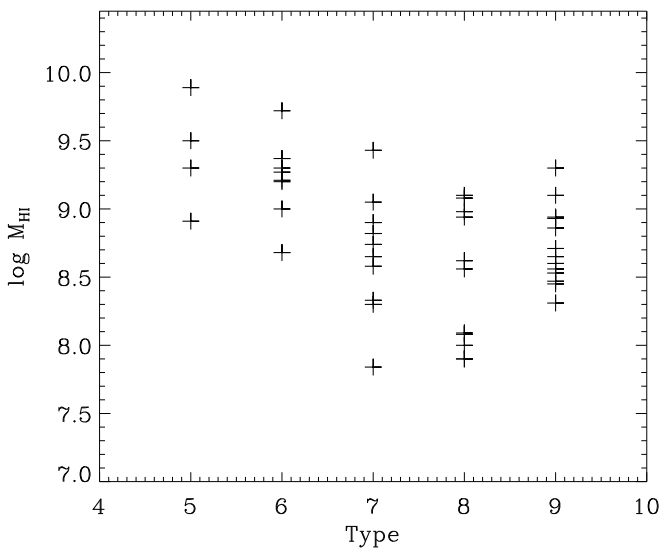
log $M_{HI}$
10.0
9.5
9.0
8.5
8.0
7.5
7.0
4
5
6
7
8
9
10
Type

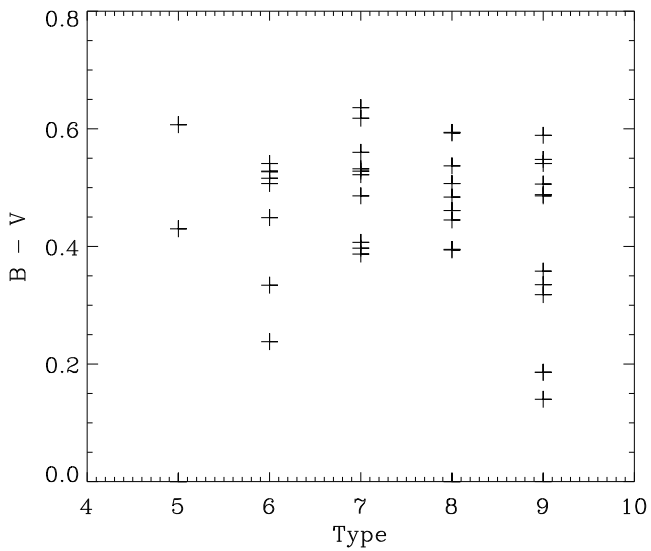
B − V
0.8
0.6
0.4
0.2
0.0
4
5
6
7
8
9
10
Type

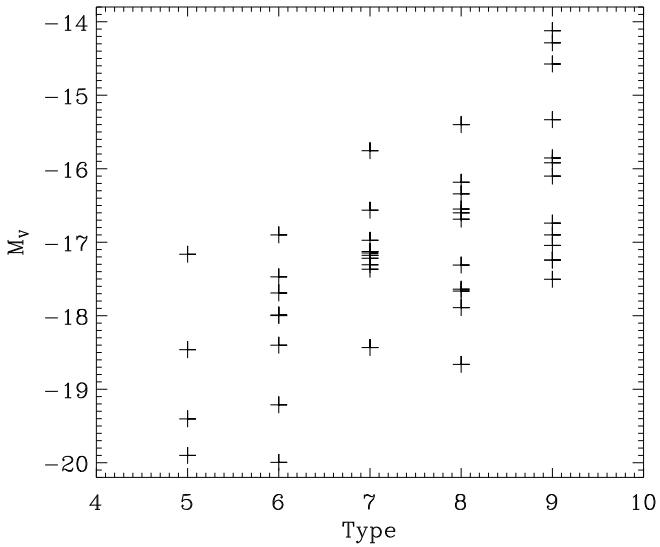
$M_V$
−14
−15
−16
−17
−18
−19
−20
4
5
6
7
8
9
10
Type